The Journal of Physiology

Functional characterization of Atlantic salmon (*Salmo salar* L.) PepT2 transporters

Francesca Vacca[1], Ana S. Gomes[2], Koji Murashita[3], Raffella Cinquetti[1], Cristina Roseti[1], Amilcare Barca[4], Ivar Rønnestad[2], Tiziano Verri[4] and Elena Bossi[1]

[1]*Laboratory of Cellular and Molecular Physiology, Department of Biotechnology and Life Sciences, University of Insubria, Varese, Italy*
[2]*Department of Biological Sciences, University of Bergen, Bergen, Norway*
[3]*Research Center for Aquaculture Systems, National Research Institute of Aquaculture, Japan Fisheries Research and Education Agency, Minami-ise, Mie, Japan*
[4]*Laboratory of Applied Physiology, Department of Biological and Environmental Sciences and Technologies, University of Salento, Lecce, Italy*

Edited by: Peying Fong & Morag Mansley

Linked articles: This article is highlighted in a Perspective article by Sala-Rabanal. To read this article, visit https://doi.org/10.1113/JP283171.

The peer review history is available in the supporting information section of this article (https://doi.org/10.1113/JP282781#support-information-section).

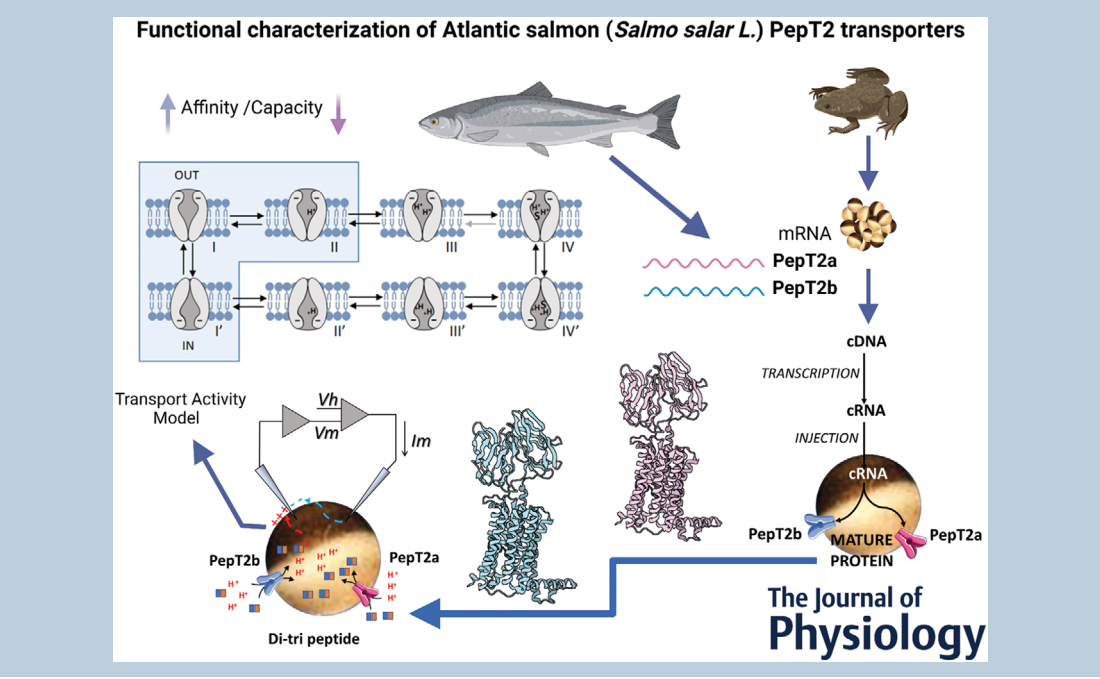

Francesca Vacca is a post-doctoral fellow at the centre of Synaptic Neuroscience and Technology at the Istituto Italiano di Tecnologia (IIT), Genoa, Italy. Currently, she works on the Hybrid Photosensitive Synapse for High resolution Vision project, supported from the Compagnia San Paolo. She got her MSc in biology from the University of Salento, Lecce, Italy (2015) and PhD from the University of Insubria, Varese, Italy (2020). There she focused on the functional characterization of membrane transport proteins through heterologous expression and electrophysiological measurements. Her research interests in the field of comparative physiology covered biophysical comparison of paralogues/orthologues to investigate their sequence/function relationship.

T. Verri and E. Bossi contributed equally to this work.

DOI: 10.1113/JP282781

Abstract The high-affinity/low-capacity system Slc15a2 (PepT2) is responsible for the reuptake of di/tripeptides from the renal proximal tubule, but it also operates in many other tissues and organs. Information regarding PepT2 in teleost fish is limited and, to date, functional data are available from the zebrafish (*Danio rerio*) only. Here, we report the identification of two *slc15a2* genes in the Atlantic salmon (*Salmo salar*) genome, namely *slc15a2a* and *slc15a2b*. The two encoded PepT2 proteins share 87% identity and resemble both structurally and functionally the canonical vertebrate PepT2 system. The mRNA tissue distribution analyses reveal a widespread distribution of *slc15a2a* transcripts, being more abundant in the brain and gills, while *slc15a2b* transcripts are mainly expressed in the kidney and the distal part of the gastrointestinal tract. The function of the two transporters was investigated by heterologous expression in *Xenopus laevis* oocytes and two-electrode voltage-clamp recordings of transport and presteady-state currents. Both PepT2a and PepT2b in the presence of Gly-Gln elicit pH-dependent and Na^+ independent inward currents. The biophysical and kinetic analysis of the recorded currents defined the transport properties, confirming that the two Atlantic salmon PepT2 proteins behave as high-affinity/low-capacity transporters. The recent structures and the previous kinetic schemes of rat and human PepT2 qualitatively account for the characteristics of the two Atlantic salmon proteins. This study is the first to report on the functional expression of two PepT2-type transporters that operate in the same vertebrate organism as a result of (a) gene duplication process(es).

(Received 31 January 2022; accepted after revision 16 March 2022; first published online 12 April 2022)
Corresponding author Elena Bossi: Laboratory of Cellular and Molecular Physiology, Department of Biotechnology and Life Sciences, University of Insubria, Via J.H.Dunant3 Varese 21100, Italy. Email: elena.bossi@uninsubria.it

Abstract figure legend Two genes coding for high-affinity/low-capacity system Slc15a2 (PepT2), are present in the Atlantic salmon (*Salmo salar*) genome: *slc15a2a* and *slc15a2b*. The two encoded PepT2 proteins share 87% identity and resemble both structurally and functionally the canonical vertebrate PepT2 system. Heterologous expression in Xenopus laevis oocytes and two-electrode voltage-clamp were applied to record transport and presteady-state currents to characterize the function of the two transporters. The transport properties collected confirmed that the previous kinetic schemes of rat and human PepT2 qualitatively account for the characteristics of the two Atlantic salmon proteins. This study is the first to report on the functional expression of two PepT2-type transporters that operate in the same vertebrate organism as a result of (a) gene duplication process(es).

Key points

- Two *slc15a2*-type genes, *slc15a2a* and *slc15a2b* coding for PepT2-type peptide transporters were found in the Atlantic salmon.
- *slc15a2a* transcripts, widely distributed in the fish tissues, are abundant in the brain and gills, while *slc15a2b* transcripts are mainly expressed in the kidney and distal gastrointestinal tract.
- Amino acids involved in vertebrate Slc15 transport function are conserved in PepT2a and PepT2b proteins.
- Detailed kinetic analysis indicates that both PepT2a and PepT2b operate as high-affinity transporters.
- The kinetic schemes and structures proposed for the mammalian models of PepT2 are suitable to explain the function of the two Atlantic salmon transporters.

Introduction

The solute carrier 15 (Slc15) family includes H^+-dependent transporters traditionally divided into peptide transporters and peptide/histidine transporters, all known for their key role in the cellular uptake/reuptake of di/tripeptides and peptidomimetics (Smith et al., 2013; Viennois et al., 2018; Zhao & Lu, 2015). The peptide transporter sub-group includes two transport systems: the low-affinity/high-capacity system Slc15a1 (PepT1), mainly expressed in the brush border membrane (BBM) of the small intestinal enterocytes, and the high-affinity/low-capacity system Slc15a2 (PepT2). PepT2 was initially discovered as the peptide transporter of the BBM of the renal proximal tubular cell but has

been shown to be widely distributed in (epithelial and non-epithelial cells of) many other organs and tissues including the central nervous system, the choroid plexus, the enteric nervous system, lung, skin, intestine, glands, testis, prostate, ovary, uterus and eye (Biegel et al., 2006; Ruhl et al., 2005). First cloned from human kidney in 1995 (Liu et al., 1995), PepT2 was later well described in several mammalian species. In terms of function, detailed electrophysiological data for the transporter were first reported for rabbit (Boll et al., 1996), and then for rat (Wang et al., 1998), human (Chen et al., 1999; Sala-Rabanal et al., 2008) and mouse (Rubio-Aliaga et al., 2000). In parallel, a very large number of di/tripeptides, peptidomimetics and peptide-like drugs have been tested and shown to be substrates of the mammalian PepT2 transporters (reviewed in, e.g. Smith et al., 2013; Viennois et al., 2018; Zhao & Lu, 2015).

Despite the increased interest in piscine di/tripeptide transporters in recent years, mainly due to their role in digestive and absorptive physiology, growth and nutrition (see, e.g. Romano et al., 2014; Verri et al., 2010; Verri et al., 2011; Verri et al., 2017), functional data on PepT2 are still missing, except for the zebrafish (*Danio rerio*) (Romano et al., 2006). Based on the zebrafish data, piscine PepT2 operates as a 'canonical' low-capacity/high-affinity transporter and is mainly expressed in the kidney, brain and intestine, but it is also present in the gills, eye and skeletal muscle (Romano et al., 2006). Later studies in other teleost fish species, mostly of commercial interest, have shown that PepT2 is present in the intestine, specifically confined to the mid-to-distal part and mainly located at the BBM of the enterocytes (see, e.g. Con et al., 2017). Probably, this is to support the absorption of (residual) luminal di/tripeptides that reach the terminal gut region (summarized in Table 1).

In this paper, we report the characterization of two newly identified PepT2-type proteins in the Atlantic salmon (*Salmo salar*, L.). Both transporters structurally and functionally resemble the mammalian PepT2 paradigm, thus differing from the two PepT1-type proteins previously described in salmon (Gomes et al., 2020; Ronnestad et al., 2010). The kinetic properties of the two Atlantic salmon PepT2 transporters have been explored by expressing the proteins in *Xenopus laevis* oocytes and then analysed by two-electrode voltage-clamp recordings of the transport current (I_t) and the presteady-state current (I_{PSS}). The presence of their mRNAs has also been analysed in several target tissues. To our knowledge, this is the first report that focuses on two *slc15a2* (paralogue) genes in a vertebrate species, a result of the specific salmonid whole-genome duplication (WGD) event, and that comparatively accesses the kinetics of two highly similar PepT2 transporters belonging to the same genetic background.

Materials and methods

Ethics statement

The research using Atlantic salmon was conducted in accordance with the Norwegian Animal Welfare Act of 12 December 1974, no. 73, § 22 and § 30, amended 19 June 2009, and all handling and procedures related to fish described in this study have been approved by the National Animal Research Authority in Norway (Fots ID 14984). The Cargill Innovation Centre (Dirdal, Norway) facility has a general permission to conduct fish experiments, licence number 2016/2835 (24 February 2016) provided by the Norwegian Food Safety Authority.

The research involving *Xenopus laevis* oocytes was conducted using an experimental protocol approved locally by the Committee of the *'Organismo Preposto al Benessere degli Animali'* of the University of Insubria (OPBA permit no. 02_15) and by the Italian Ministry of Health (permit no. 1011/2015).

The investigators understand the ethical principles under which the journal operates and declare that their work complies with the journal's animal ethics checklist.

Animals and tissue collection

Atlantic salmon were reared (Cargill Innovation Centre, Dirdal, Norway) following standard procedures, in seawater at 8.7°C with a stock density below 25 kg fish/m^3 and constant daylight. The fish were fed a commercial EWOS 10 mm pellet size diet (for information regarding diet composition please refer to Gomes et al., 2020) using automatic feeders three times a day (22:00–24:00, 02:00–04:00, 06:00–08:00). Atlantic salmon (906 ± 122 g wet weight; 38.8 ± 1.8 cm total length; $n = 8$) were collected 2 h after the 06:00–08:00 meal and killed with an overdose of MS222 (tricaine methansulfonate 300 mg l^{-1}; Norsk Medisinaldepot AS, Bergen, Norway) on site. The selected tissues were rapidly collected, snap-frozen in liquid nitrogen and stored at −80°C until further analysis.

Molecular cloning

Total RNA was extracted from the hindgut and whole brain of Atlantic salmon using TRI Reagent (Millipore Sigma, St. Louis, MO, USA) following the manufacturer's instructions. To avoid contamination with genomic DNA, total RNA was treated with TURBO DNA-free kit (Thermo Fisher Scientific, Waltham, MA, USA) according to the manufacturer's protocol, and 1.5 μg of DNase-treated RNA was used to synthesize cDNA using SuperScript III First-Strand Synthesis system for RT-PCR kit (Thermo Fisher Scientific) with Oligo $(dT)_{20}$ primers according to the manufacturer's protocol.

Table 1. Organ/tissue distribution of *slc15a2* mRNA in teleost fish

Order	Species	GenBank Acc. No.	Developmental stage	Tissue distribution	References
Cypriniformes	*Danio rerio* (zebrafish)	DQ192597[&,$], NM_0 010 39828[&]	Embryo/larva (1–7 dpf)	Brain, otic vesicle	Romano et al., 2006; Santos et al., 2020
			Adult	Intestine, kidney, brain, eye, gills, skeletal muscle, spleen	
	Cyprinus carpio (common carp)	DC997173	Juvenile	Intestine	Ostaszewska et al., 2010
	Tor putitora (golden mahseer)	NS	Adult	Brain, trunk kidney, liver, muscle, gills, intestine, head kidney, spleen	Barat et al., 2016
	Megalobrama amblycephala (blunt snout bream *alias* Wuchang bream)	NS	Juvenile	Liver	Ahmed et al., 2019
	Carassius auratus gibelio (gibel carp *alias* silver crucian carp)	NS	Juvenile	Liver	Ji et al., 2021
Cichliformes	*Oreochromis niloticus* (Nile tilapia)	XM_0 054 75385	Juvenile	Proximal, mid and distal intestine, stomach, kidney, liver, gills, brain, spleen, muscle	Huang et al., 2015; Chourasia et al., 2018
	Oreochromis mossambicus (Mozambique tilapia)	KX034111	Larva (3–14 dpf)	NA	Chourasia et al., 2018; Con et al., 2017; Con et al., 2019; Con et al., 2021
			Adult	Proximal, mid and distal intestine, kidney, muscle, liver, brain, pituitary, skin, stomach, spleen, heart, fat, gills, oesophagus	
Perciformes	*Dicentrarchus labrax* (European seabass)[†]	NS	Juvenile	Intestine	Kokou et al., 2019
Pleuronectiformes	*Scophthalmus maximus* (turbot)	NS	Juvenile	Proximal, mid and distal intestine, pyloric caeca, stomach, rectum, muscle	Xu et al., 2016; Xu et al., 2017

Data were obtained by quantitative real-time polymerase chain reaction, except for [&] where semi-quantitative reverse transcriptase polymerase chain reaction (embryo/larva and adult) and for [$] where *in situ* hybridization (embryo/larva) were performed; [†]recently classified in Eupercaria incertae sedis; dpf, days post-fertilization; NS not specified (only primer pair reported); NA, not assessed.

Table 2. Sequence of the specific primers used for cloning and quantitative RT-PCR (qPCR) mRNA expression analysis. Sequence accession number, primer sequences, amplicon sizes, R^2 and qPCR efficiency are indicated for each primer pair

Gene	GenBank Acc. No.	Sequence (5′→3′)	Amplicon (bp)	R^2	Efficiency (%)
Cloning					
slc15a2a	XM_01 416 5384.1	F: ATGGGGAAACGAAAGGAGCTGA R: CTACATCTTGGTGCTCTTCTCTATT	2166		
slc15a2b	XM_01 417 3652.1	F: ATGGAGACACGAAAGGAACATGA R: CTACATCTTAGTGCTCTTCTCTAT	2187		
qPCR					
β-actin	NM_0 011 23525.1	F: CCAAAGCCAACAGGGAGAAG R: AGGGACAACACTGCCTGGAT	91	0.9997	99.89
slc15a2a	XM_01 416 5384.1	F: GGGGGACACAACAAGACCAT R: CCGCGTGTTTATGAACCTCA	198	0.9983	98.52
slc15a2b	XM_01 417 3652.1	F: GGATCAGTGGATGGAGTTCCTG R: TCTGGTTCTTTTTCAAGTTGTCTTC	170	0.9976	92.47

Atlantic salmon *slc15a2a* and *slc15a2b* transcripts were identified using the zebrafish PepT2 nucleotide sequence (GenBank Acc. No. NM_001039828.1) as a query against the Atlantic salmon genome database available in GenBank, and specific primers were designed (Table 2, searches in the database performed in 2019). The complete coding sequences (CDS) of *slc15a2a* and *slc15a2b* were amplified using Q5 High-Fidelity DNA polymerase (New England Biolabs, Ipswich, MA, USA) according to the manufacturer's protocol. The following thermal program: 98°C for 30 s; 35 cycles of 98°C for 10 s, 64°C for 20 s, 72°C for 2 min; and a final step at 72°C for 2 min was used in a GeneAmp PCR system 2700 thermal cycler (Applied Biosystems, Foster City, CA, USA). The PCR products were resolved on 1% (w/v) agarose gel and purified using E.Z.N.A. Gel Extraction Kit (Omega bio-tek, Inc, Norcross, GA, USA). *slc15a2b* was cloned into a StrataClone blunt PCR cloning vector pSC-B (Agilent Technologies, Palo Alto, CA, USA), while an additional step which added 3'A overhangs to the *slc15a2a* purified PCR product was performed using Taq DNA polymerase (New England Biolabs) before cloning into pCR4-TOPO vector (Thermo Fisher Scientific). Sequencing was performed at the University of Bergen Sequencing Facility (Bergen, Norway) and sequence identity confirmed by tBLASTx analysis against the Atlantic salmon genome database available in GenBank. Furtherly, Atlantic salmon PepT2 amino acid sequences were deduced using the Expasy translate tool (https://web.expasy.org/translate/). Putative transmembrane domains were drawn using the rat PepT2 annotation data at the UniProt database (UniProtKB Acc. No. Q63424). Potential *N*-glycosylation sites were predicted using NetNGlyc 1.0 server (http://www.cbs.dtu.dk/services/NetNGlyc/) and the PTR2 family proton/oligopeptide symporter signature was defined using the ScanProsite tool (de Castro et al., 2006).

Quantitative real-time PCR (qRT-PCR)

Total RNA was isolated from the brain, gills, olfactory cavity, lip, tongue, several sections of the gastrointestinal tract (oesophagus, anterior and posterior stomach, pyloric caeca, anterior midgut, midgut, posterior midgut, and anterior and posterior hindgut), kidney and head kidney, as described above. Total RNA was treated with TURBO DNA-free (Thermo Fisher Scientific) as described above and RNA integrity assessed in all samples using an Agilent 2100 Bioanalyzer (Agilent Technologies). cDNA was synthesized as described in the section above.

Specific primers for the target transcripts and the reference gene β-actin (GenBank Acc. No. NM_001123525.1) were designed using primer-BLAST (Ye et al., 2012) (Table 2). qPCR reactions were carried out in duplicate with a final reaction volume of 20 μl using iTaq Universal SYBR Green Supermix (Bio-Rad, Hercules, CA, USA). The following qPCR conditions: 95°C for 30 s; 40 cycles of 95°C for 5 s, 60°C for 25 s, were used in a CFX 96TM Real Time System (Bio-Rad). Melting curve analysis over a range of 65 to 95°C (increments of 0.5°C for 2 s) allowed detection of non-specific products and/or primer dimers. The assay efficiency was determined using a 10-fold dilution curve of the target gene cloned in the pCR4-TOPO vector (Thermo Fisher Scientific). The qPCR efficiency varied between ∼92% and ∼100% with $R^2 > 0.99$ (Table 2).

The target transcripts and β-actin copy number were calculated for each sample based on the respective standard curve, using the following expression: Copy number = (Ct - intercept) × $(\text{slope})^{-1}$. The target transcript copy number was divided by the ng of total RNA used in the reaction and subsequently normalized with the β-actin copy number/ng of total RNA. Data were analysed and figures prepared in R version 4.0.2 (Team, 2009) using the Tidyverse package (Wickham et al., 2019).

Phylogeny and synteny analysis

The deduced mature protein sequences of Atlantic salmon PepT2a (GenBank Acc. No. XP_014020859.1) and PepT2b (GenBank Acc. No. XP_014029127.1), zebrafish PepT2 (UniProtKB Acc. No. B0S6T2), rat PepT2 (UniProtKB Acc. No. Q63424) and human PepT2 (UniProtKB Acc. No. Q16348) were aligned using ClustalX 2.1 with the default parameters (Gonnet series matrix, Gap opening penalty 10, Gap extension 0.2) and the percentages of similarity/identity between sequences were calculated using GeneDoc software (https://genedoc.software.informer.com/2.7/).

For phylogenetic analysis of the PepT2 family members, alignments were performed in MEGA X (Kumar et al., 2018) using MUSCLE with the default parameters (UPGMA clustering method, Gap opening penalty −2.90, Gap extension 0.0). The sequence alignment was analysed for the best-fit substitution model in MEGA X to select the best statistical model to study protein family evolution. The phylogenetic tree was constructed using maximum likelihood with a Jones-Taylor-Thornton model (Jones et al., 1992) with fixed Gamma distribution parameter with five rate categories and 1000 bootstrap replicates. Included in the analysis were the PepT2 sequences from four salmonids (Atlantic salmon, rainbow trout (*Oncorhynchus mykiss*), chinook salmon (*Oncorhynchus tshawytscha*) and Arctic char (*Salvelinus alpinus*)), two cyprinids (zebrafish and goldfish (*Carassius auratus*)), medaka (*Oryzias latipes*), Nile tilapia (*Oreochromis niloticus*), turbot, Atlantic herring (*Clupea harengus*), cavefish (*Astyanax mexicanus*), the primitive freshwater ray-finned fish spotted gar (*Lepisosteus oculatus*) and human (*Homo sapiens*).

The gene environment of Atlantic salmon *slc15a2* genes was characterized and compared with the homologue *slc15a2* genome region in northern pike and zebrafish. The genes flanking *slc15a2* were identified using the annotation provided by direct Genomicus genome browser consulting (https://www.genomicus.biologie.ens.fr/genomicus).

Protein modelling

SWISS-MODEL (Waterhouse et al., 2018) (https://swissmodel.expasy.org/interactive) was used to predict the structure of the Atlantic salmon PepT2a and PepT2b proteins using their primary sequences (GenBank Acc. Nos.: XP_014020859.1 and XP_014029127.1, respectively). The rat PepT2 (Protein Data Bank Acc. No.: 7nqk.1) (Parker et al., 2021) and human PepT2 (Protein Data Bank Acc. No.: 7pmy.1) (Killer et al., 2021) were used as templates to build the models. The final three-dimensional structures were visualized using SWISS-MODEL view tools.

Expression in *Xenopus laevis* oocytes and electrophysiology

The complete open reading frame encoding for Atlantic salmon PepT2a and PepT2b was subcloned into pSPORT1 plasmid. Sequence analysis confirmed a 99% identity of PepT2a to the publicly available sequence (GenBank Acc. No. XM_014165384.1; two nucleotides change, and one of these alters Leu to Ser in position 9; see Fig. 1*A*) and a 100% identity of PepT2b to the published sequence (GenBank Acc. No. XM_014173652.1).

To improve the expression in the membrane of *Xenopus laevis* oocytes, a 3' UTR sequence of 1725 bp containing two poly-adenylation signals and a poly(A) tail from rat divalent metal transporter 1 (rDmt1, *alias* rat *Slc11a2*; GenBank Acc. No. NM_013173.2) (Buracco et al., 2015) was added to the end of each Atlantic salmon PepT2 CDS.

Xenopus laevis oocytes were collected under anaesthesia (MS222; 0.10% (w/v) solution in tap water) by laparotomy from adult females (Envigo, San Pietro al Natisone, Italy) and prepared as described previously (Bossi et al., 2007). *Xenopus laevis* frogs were maintained according to international guidelines (Delpire et al., 2011; McNamara et al., 2018). In brief, the frogs were kept in a XenoPlus amphibian system, with a continuous recirculating water system (Tecniplast, Buguggiate, Varese, Italy), and a daylight cycle of 12 h. They were fed *ad libitum* with a *Xenopus* diet (Mucedola, Settimo Milanese, Milan, Italy). The oocytes were collected three times from each frog, and the animals were killed with an overdose of anaesthetic (0.5% (w/v) MS222) after the third oocyte collection (Torreilles et al., 2009).

Capped cRNAs of the two Atlantic salmon PepT2 were synthesized by *in vitro* transcription using T7 RNA polymerase from cDNAs in pSPORT1 linearized with NotI and purified with Wizard SV Gel and PCR clean-up system (Promega Italia, Milan, Italy). The purified cRNAs were quantified by NanoDrop 2000 Spectrophotomer (Thermo Fisher Scientific), and 12.5 ng injected into the oocytes using a manual microinjection system (Drummond Scientific Company, Broomall, PA, USA). Before electrophysiological studies, the cRNA-injected oocytes were incubated at 18°C for 3–4 days in NDE (NaCl 96 mmol l^{-1}, KCl 2 mmol l^{-1}, $CaCl_2$ 1.8 mmol l^{-1}, $MgCl_2$ 1 mmol l^{-1}, Hepes 5 mmol l^{-1}, pyruvate 2.5 mmol l^{-1} and gentamycin sulphate 0.05 mg ml^{-1} pH 7.6).

Two-electrode voltage-clamp experiments were performed using a commercial amplifier (Oocyte Clamp OC-725B, Warner Instruments, Hamden, CT, USA) and the pCLAMP software (Version 10.7, Molecular Devices, San Jose CA, CA, USA).

The holding potential was kept at −60 mV; the voltage pulse protocol consisted of 10 square pulses from −140 to +20 mV (20 mV increments) of 400 ms each. Signals were filtered at 0.1 kHz, sampled at 0.2 or 0.5 kHz, and

1 kHz. transport-associated currents (I_{tr}) were calculated by subtracting the traces in the absence of substrate from those in its presence. When the normalization is reported, the values of the steady-state currents were divided by the value of the current recorded for each transporter at −140 mV in the presence of 1 mmol l^{-1} Gly-Gln at pH 7.6. The number of samples n corresponds to the number of oocytes used in each condition and the batches correspond to the animals from which the oocytes were collected. These data are summarized in the figure captions.

Solutions

The external control solution had the following composition: NaCl 98 mmol l^{-1}, $MgCl_2$ 1 mmol l^{-1}, $CaCl_2$ 1.8 mmol l^{-1}. For pH 5.5 and 6.5 the buffer solution Pipes 5 mmol l^{-1} was used, for pH 7.6, Hepes 5 mmol l^{-1}. Final pH values were adjusted with HCl or NaOH. The substrate oligopeptide Gly-Gln (Sigma-Aldrich) was added at the indicated concentrations (from 3 μmol l^{-1} to 3 mmol l^{-1}) in the solutions with appropriate pH.

Data analysis, statistics and figure preparation

Steady-state transport currents from substrate dose–response experiments were fitted with the Michaelis-Menten equation, eqn (1):

$$\left[I_0 = \frac{-I_{max}}{1 + ([S]/K_{0.5})} + I_{max} \right] \quad (1)$$

for which I_0 is the evoked current, I_{max} is the derived relative maximal current, S is the substrate (Gly-Gln) concentration and $K_{0.5}$ is the substrate concentration at which current is half-maximal.

To analyse the presteady-state currents, the current traces were fitted with a double-exponential function (2):

$$\left[I_t = I_m e^{\left(-\frac{t}{\tau_m}\right)} + I_{PSS} e^{\left(-\frac{t}{\tau_{PSS}}\right)} + I_{SS} \right] \quad (2)$$

where I_t is the total current across the oocyte membrane; t is the time; I_m is a capacitive current with time constant τ_m associated with the oocyte plasma membrane, I_{PSS} is a transient current associated with the transporter expression with time constant τ, and I_{SS} is the steady-state current. At each voltage, the amount of displaced charge (Q) was calculated by integrating the isolated traces after zeroing any residual steady-state transport current. Finally, the charge *vs.* voltage relationship (Q/V) was fitted with the Boltzmann equation, eqn (3):

$$\left[Q = \frac{Q_{max}}{1 + e^{[-(V - V_{0.5})/\sigma]}} \right] \quad (3)$$

where Q_{max} is the maximal moveable charge, $V_{0.5}$ is the voltage at which half of the charge is moved (that is, the midpoint of the sigmoidal), and $\sigma = kT/q\delta$ represents a slope factor, in which q is the elementary electronic charge, k is the Boltzmann constant, T is the absolute temperature, and δ is the fraction of electrical field over which the charge movement occurs.

Data were analysed using Clampfit 10.7 (Molecular Devices). All figures and statistics were prepared with Origin 8.0 (OriginLab, Northampton, MA, USA).

Figures 4, 5 and 7 show descriptive statistical data plotted as means (SD), in Fig. 6 the statistical analysis compares different pH conditions for each transporter and between transporters at the same pH of the data in Fig. 5. The comparison was done by applying the two-sample t test or Mann-Whitney's U test. The detailed statistical values are reported in the statistical summary document.

Results

Sequence and comparative analysis

Two Atlantic salmon *slc15a2* genes, namely *slc15a2a* (GenBank Acc. No. XM_014165384.1) and *slc15a2b* (GenBank Acc. No. XM_014173652.1), were identified in the GenBank database (Table 1). The two paralogues (*slc15a2a* and *slc15a2b*) encoded for proteins of 721 and 728 amino acids, respectively. PepT2a (GenBank Acc. No. XP_014020859.1) and PepT2b (GenBank Acc. No. XP_014029127.1) shared 93% similarity and 87% identity at the amino acid level. Comparative hydropathy analysis predicted 12 potential transmembrane domains with a large extracellular loop between transmembrane domains IX and X (Fig. 1*A*). The structural key motif PTR2 family proton/oligopeptide symporter signature (orange diamonds, Fig. 1*A*) was well conserved in the Atlantic salmon PepT2 sequences, as well as the potential *N*-glycosylation site at the extracellular surface (brown circle, Fig. 1*A*).

When the sequences of the Atlantic salmon PepT2a and PepT2b were analysed for conserved functional residues (Killer et al., 2021), the proton and peptide binding sites (blue triangles, Fig. 1*A*), the amino acids that form the extracellular gate (green triangles, Fig. 1*A*) and the intracellular salt bridge (red triangles, Fig. 1*A*), as well as the amino acids involved in the subsequent steps of the transport cycle (1–5, Fig. 1*A*), were conserved if compared not only with the mammalian PepT2 but also with mammalian and piscine PepT1 transporters. Notably, when compared with the rat ('outward-facing open' conformation) and human ('inward-facing partially occluded' conformation; substrate bound) PepT2 structures, Atlantic salmon PepT2a and PepT2b proteins both shared ∼55% identity with their mammalian counterparts (Fig. 1*B*). Moreover, as emerged from the

A

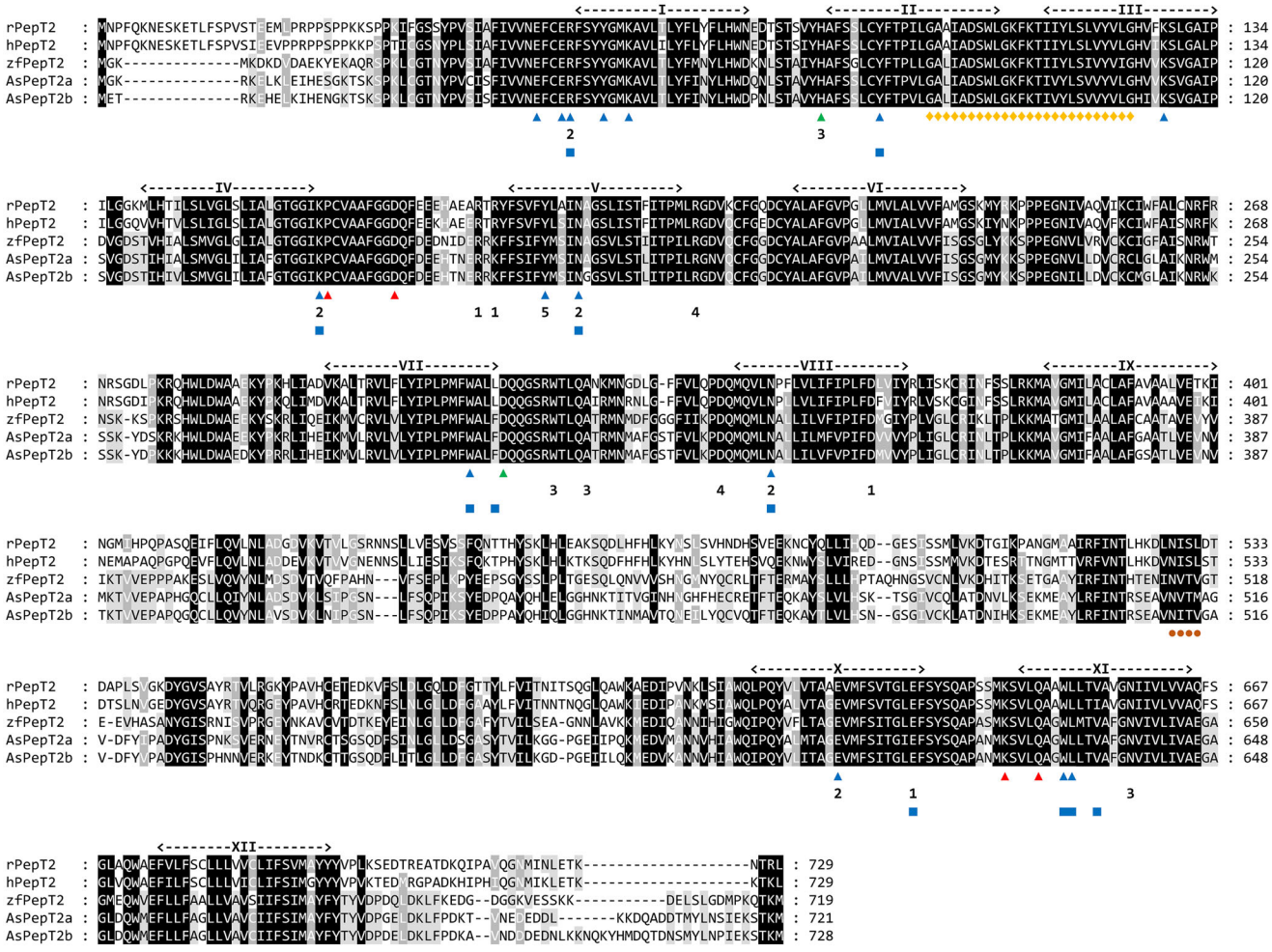

Key residues

I-XII	‘putative transmembrane domain’
◆	‘PTR2 family proton/oligopeptide symporter signature 1’
●	‘extracellular N-glycosylation site’
▲	‘extracellular gate’
▲	‘intracellular salt bridge’
▲	‘peptide binding’
1	‘outward-facing open’ state (apo)
2	‘outward-facing open’ state (substrate-bound)
3	‘outward-facing occluded’ state (substrate-bound)
4	‘inward-facing partially occluded’ state (substrate-bound)
5	‘inward-facing open’ state (apo)
■	‘substrate recognition’

Figure 1. Aligments and three dimensional rappresentations of Pept2 proteins
A, multiple alignments of the Atlantic salmon PepT2a (AsPepT2a) and PepT2b (AsPepT2b), zebrafish PepT2 (zfPepT2), rat PepT2 (rPepT2) and human (hPepT2) amino acid sequences as obtained by using ClustalX 2.1 and edited in GeneDoc 2.7 software. The conserved PTR2 family proton/oligopeptide symporter signature 1 (PROSITE pattern PS01022 – amino acid residues 100–124 on rPepT2 and hPepT2, and 86–110 on zPepT2, AsPepT2a and AsPepT2b) is marked by orange diamonds (◊). The putative transmembrane domains, named I to XII, were drawn using the annotation data of rPepT2 (see UniProtKB Acc. No. Q63424). Only one conserved extracellular *N*-glycosylation site (PROSITE pattern PS00001 – amino acid residues 528–532 on rPepT2 and hPepT2, 513–516 on zPepT2, and 511–514 on AsPepT2a and AsPepT2b), as obtained using NetNGlyc 1.0 server, is reported and marked by brown circles (●). Highlighted are key residues referring to the ‘extracellular gate’ (green triangles, ▲), ‘intracellular salt bridge’ (red triangles, ▲), and ‘peptide binding’ (blue triangles, ▲), as defined on the Cryo-EM structure of the rat PepT2 transporter (Protein Data Bank Acc. No. 7nqk.1; Parker et al., 2021). Key residues

analysis of the superposed structures, (besides the large extracellular loop regions) little areas of 'low consistency' (red) amongst large areas of 'high consistency' (green) could be defined along the sequence, including some located within the transmembrane domains and others located at the basis of the extracellular loop stem (for details, see Fig. 1*B*).

Phylogenetic analysis of the putative Atlantic salmon PepT2a and PepT2b showed that these two proteins clustered into two distinct branches with their salmonid homologue sequences (Fig. 2). Northern pike PepT2 was the closest relative to the salmonid clade, and except for goldfish, which also underwent an additional WGD, only one PepT2-type protein was found in other teleost species.

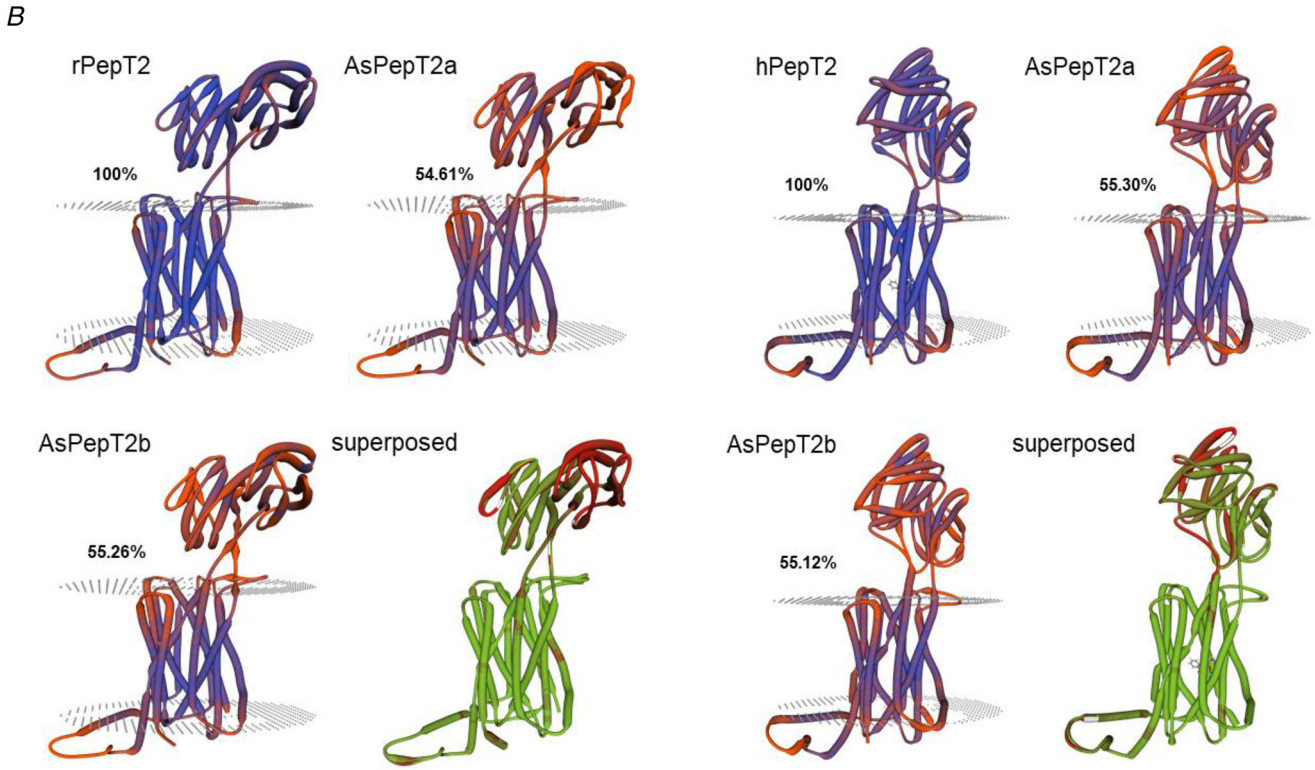

Figure 1. Continued

referring to the mechanism for substrate recognition and transport, as defined on the Cryo-EM structure of the human PepT2 (Protein Data Bank Acc. No. 7pmy.1) or human PepT1 (Protein Data Bank Acc. Nos. 7pn1.1, 7pmx.1 and 7pmw.1; Killer et al., 2021) are also highlighted. Amino acid residues involved in the subsequent steps of the transport cycle are shown: 'outward-facing open' state (apo) (1) (adapted from the human PepT1 structure, ref. Protein Data Bank Acc. No. 7pn1.1), 'outward-facing open' state (substrate-bound), (2) (adapted from the human PepT1 structure, ref. Protein Data Bank Acc. No. 7pmx1.1), 'outward-facing occluded' state (substrate-bound), (3) (adapted from the human PepT1 structure, ref. Protein Data Bank Acc. No. 7pmw1.1), 'inward-facing partially occluded' state (substrate-bound), (4) (adapted from the human PepT2 structure, ref. Protein Data Bank Acc. No. 7pmy1.1), 'inward-facing open' state (apo), (5) (from the human PepT1 Alphafold structure prediction, ref. Alphafold Acc. No. AF-P46059-F1; Jumper et al., 2021). The amino acid residues involved in 'substrate recognition' are all specifically indicated, marked by blue squares (■) (from the human PepT2 structure, ref. Protein Data Bank Acc. No. 7pmy1.1). Substrate: Ala-Phe. For details on transport dynamics, mechanism, states and conformations, please see Killer et al. (2021). *B*, three-dimensional representation of single and superposed structures of rPepT2, AsPepT2a and AsPepT2b ('outward-facing open' conformation) (left), and hPepT2, AsPepT2a and AsPepT2b ('inward-facing partially occluded' conformation) (substrate-bound; the substrate Ala-Phe is represented) (right), as obtained by using SWISS-MODEL tools. The models were built using as a template the rPepT2 (Protein Data Bank Acc. No. 7nqk.1) or the hPepT2 (Protein Data Bank Acc. No. 7pmy.1); then, the models were superposed by using the 'Compare' view tool. Colour schemes for single structures based on (model) confidence (it evaluates, for each residue of the model, the expected similarity to the native structure, thus representing an index of the 'local quality' of the residue): red, low confidence and blue, high confidence. Colour scheme for superposed structures based on consistency (it identifies local deviations of a protein structure from the 'consensus' established by all other structures selected for comparison): red, low consistency and green, high consistency. Percentage identities of Atlantic salmon PepT2 proteins *vs*. the rat (left) and human (right) PepT2 proteins are reported. [Colour figure can be viewed at wileyonlinelibrary.com]

The Atlantic salmon *slc15a2a* gene maps to chromosome ssa21 and the *slc15a2b* gene to chromosome ssa25. Both *slc15a2* paralogues share a conserved gene environment, with a total of eight neighbouring genes upstream (out of 10) and six genes downstream (out of 10) being syntenic (Fig. 3). The conservation of synteny is particularly evident in the upstream region of *slc15a2*. The Atlantic salmon *slc15a2a* upstream region shares 10 and nine (out of 10) genes with the Northern pike and zebrafish homologue region, respectively, while for *slc15a2b* 8 genes are conserved in the Northern pike and zebrafish upstream homologue region. The genomic region downstream *slc15a2* is also conserved but to a lesser extent: salmon *slc15a2a* shares five and three genes with the Northern pike and zebrafish, respectively, while *slc15a2b* shares eight genes with the Northern pike, but no genes are conserved in the downstream area with the zebrafish homologue region.

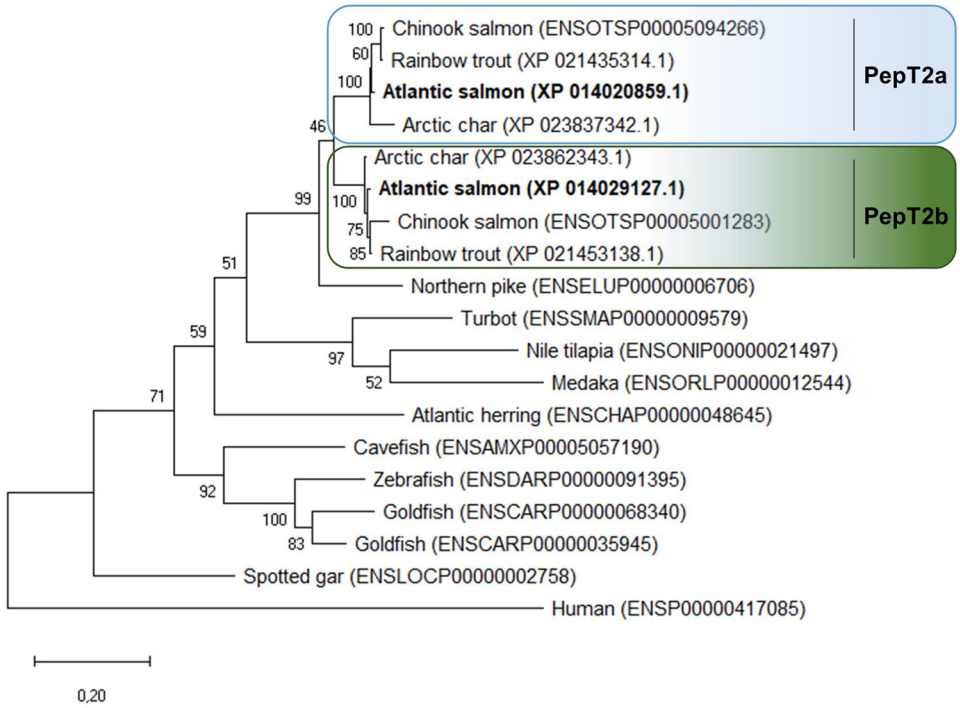

Figure 2. Phylogenetic relationship of fish and mammalian PepT2 based on predicted protein sequences
The (unrooted) phylogenetic tree was constructed based on deduced PepT2 amino acid sequences using the maximum likelihood method, 1000 bootstrap replicates, and Jones-Taylor-Thornton + G matrix-based model in MEGA X. The percentage of trees in which the associated taxa clustered together is shown next to the branches. Protein Acc. Nos. for GenBank or Ensembl databases are provided next to species common name. [Colour figure can be viewed at wileyonlinelibrary.com]

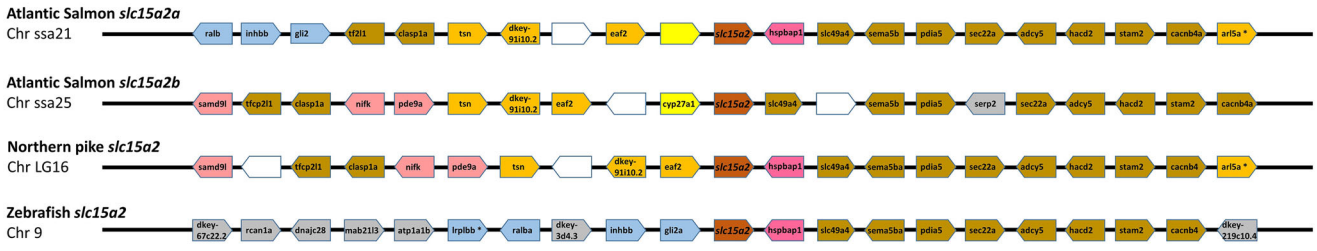

Figure 3. Synteny analysis of *slc15a2* genomic region in teleosts
From top, *slc15a2a* and *slc15a2b* genes from Atlantic salmon (*Salmo salar*), *slc15a2* from Northern pike (*Esox lucius*) and zebrafish (*Danio rerio*). The chromosome (Chr) number is indicated below each species name. The central pentagons in dark orange indicate the *slc15a2* genes. For each *slc15a2* gene, 10 flanking genes upstream and downstream are represented by different coloured pentagons. Each colour identifies sets of orthologous genes based on the degree of conservation between species and between the chromosomes within species and white pentagons represent non-identified genes. The pentagons point in the direction of transcription and only protein-coding genes are indicated. [Colour figure can be viewed at wileyonlinelibrary.com]

Tissue distribution of Atlantic salmon *slc15a2a* and *slc15a2b*

Tissue expression analysis, focused on the Atlantic salmon head kidney and kidney (Fig. 4*A*) and the alimentary canal and head tissues (Fig. 4*B*), revealed that *slc15a2a* and *slc15a2b* have a different distribution profile. Atlantic salmon *slc15a2a* showed a wider tissue distribution profile with lower mRNA expression levels in the posterior stomach and higher levels in the brain and gills (Fig. 4*B*). Interestingly, *slc15a2b* mRNA expression was mainly restricted to the gastrointestinal tract, specifically from pyloric caeca to the posterior hindgut, and excluding the stomach (Fig. 4*B*). *slc15a2b* mRNA expression was abundant in the hindgut (Fig. 4*B*), as well as in the kidney (Fig. 4*A*).

Transport currents

In Fig. 5*A* and *C*, representative current traces recorded from oocytes expressing the two proteins are reported. At −60 mV both PepT2 paralogues are functional and elicit transport currents in the presence of 1 mmol l^{-1} Gly-Gln. The currents are larger at pH 5.5 and decrease with increasing pH, and even at pH 8.5 both proteins generate an inward current. PepT2a shows currents larger than PepT2b (Fig. 5*A*–*D* and Fig. 6). Moreover, for both PepT2a and PepT2b the current traces show an uncoupled current at acidic pH (5.5 and 6.5). These currents are visible in Fig. 5*A* and *C* by observing the position of the representative traces with respect to the dotted line, which is the zero current conventionally set at the holding potential at pH 7.6 for each transporter. This current is due to H^+ entry at the acidic pH, mainly through the heterologously expressed transporters (leakage current), but also through endogenous oocyte channels.

The behaviour of PepT2a and PepT2b at different pH and different membrane voltages was investigated by measuring the transport-associated current by applying the voltage pulse protocol described in *Materials and methods* (see Fig. 9 where the recorded traces are reported). The Atlantic salmon PepT2 protein activity is pH- and voltage dependent (Fig 5*B* and *D*) and Na^+-independent (Fig. 5*B* and *D inset*). In the presence of the substrate, the decrease of external pH has a similar effect on the two transporters: i.e. the amplitude of the currents at pH 5.5 is the largest recorded in the voltage range from −140 to −20 mV (detailed by the box plot in Fig. 6). In PepT2a, increasing the pH has more impact on the reduction of the transport-associated current. In Fig. 6*A* and *B*, the comparison of the transport currents (I_{tr}) recorded at −120 and −60 mV at the indicated pH conditions confirmed that the amplitudes recorded are significantly different.

To understand the effect of pH on the transport it is essential to investigate the kinetic parameters in the different conditions. In Fig. 7 the transport current–substrate concentration plot is reported for both PepT2 proteins at three pH values (5.5, 6.5 and 7.6). The relative maximal current (I_{max}) and the Gly-Gln apparent affinity ($1/K_{0.5}$) for each condition are given in Table 3.

The I_{max}, $K_{0.5}$ and transport efficiency are reported for PepT2a in Fig. 8*A*, *B* and *C* and for PepT2b in *D*, *E* and *F*. These parameters allow an evaluation of the

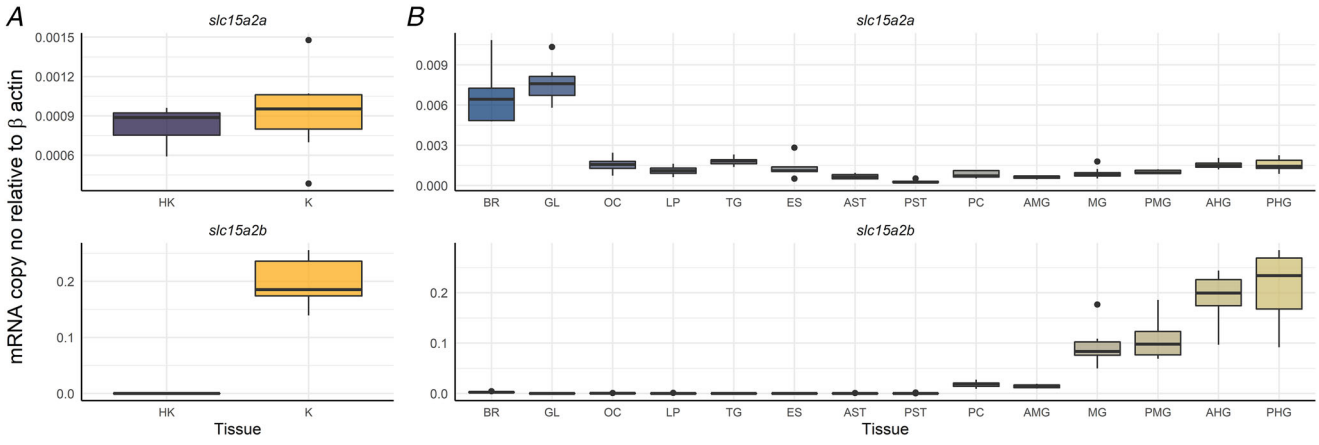

Figure 4. mRNA tissue distribution of *slc15a2a* and *slc15a2b* in head kidney and kidney (*A*) and head tissues and along the gastrointestinal tract of the Atlantic salmon (*B*) using quantitative RT-PCR
Results are shown as target *slc15a2* copy number per ng of total RNA normalized using *β-actin* copy number per ng of total RNA. The line in the boxplot indicates the median and boxes the 1st to 3rd quartiles, whiskers mark variation outside 1st and 3rd quartiles and dots the outliers (n = 8 for all tissues, except for HK, K, GL, OC, AMG, PMG and AHG where n = 7). HK, head kidney; K, kidney; BR, brain; GL, gills; OC, olfactory cavity; TG, tongue; ES, oesophagus; AST, anterior stomach; PST, posterior stomach; PC, pyloric caeca; AMG, anterior midgut; MG, midgut; PMG, posterior midgut; AHG, anterior hindgut; PHG, posterior hindgut. [Colour figure can be viewed at wileyonlinelibrary.com]

functional characteristics and the differences between the two proteins. As suggested by the I_{max} *vs.* voltage (I_{max}/V) graphs in Fig. 8*A* and *D*, the I_{max} of the two PepT2 transporters is voltage dependent, and the current amplitudes increase from 0 to −140 mV for both proteins and at all tested pH. Raising the extracellular pH from 5.5 to 7.6 results in a pronounced decrease in the maximal transport currents ∼5-fold at −60 mV (i.e. from −192.7 (20.8) nA at pH 5.5 to −39.4 (2.3) nA at pH 7.6 for PepT2a and from −69.2 (4.0) nA at pH 5.5 to −14.1 (0.5) nA at pH 7.6 for PepT2b). Notably, the I_{max} recorded for PepT2a at −60 mV is ∼3-fold higher than the I_{max} current recorded at the same membrane voltage for PepT2b, for all tested pH.

Figure 8*B* and *E* show the $K_{0.5}/V$ curves for PepT2a and PepT2b, respectively. For both transporters at all external pH conditions, $K_{0.5}$ values exhibit a peculiar dependence on membrane potentials with an increase of $K_{0.5}$ values from −60 to −140 mV. $K_{0.5}$ values are only slightly modified by the acidification of the bathing solution: at

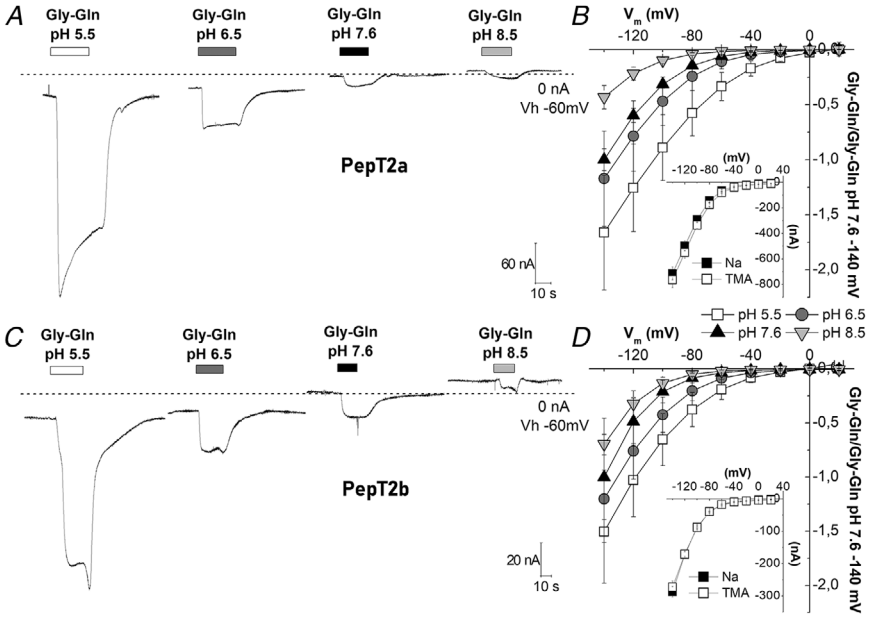

Figure 5. Transport of Gly-Gln in *Xenopus* oocytes expressing Atlantic salmon PepT2a (*A*, *B*) and PepT2b (*C*, *D*)
In *A* and *C*, representative traces (1 mmol l^{-1} Gly-Gln in NaCl solution), the dashed line represents the baseline (conventionally fixed at the value in NaCl solution at pH 7.6). *B* and *D*, current/voltage relationships (the values are the means (SD) of the current normalized to the mean value of the current at −140 mV and pH 7.6); insets, currents at pH 6.5 in the presence of 98 mmol l^{-1} NaCl or tetraethylammonium chloride. Data are means (SD) from 4–24 oocytes from 1–5 batches.

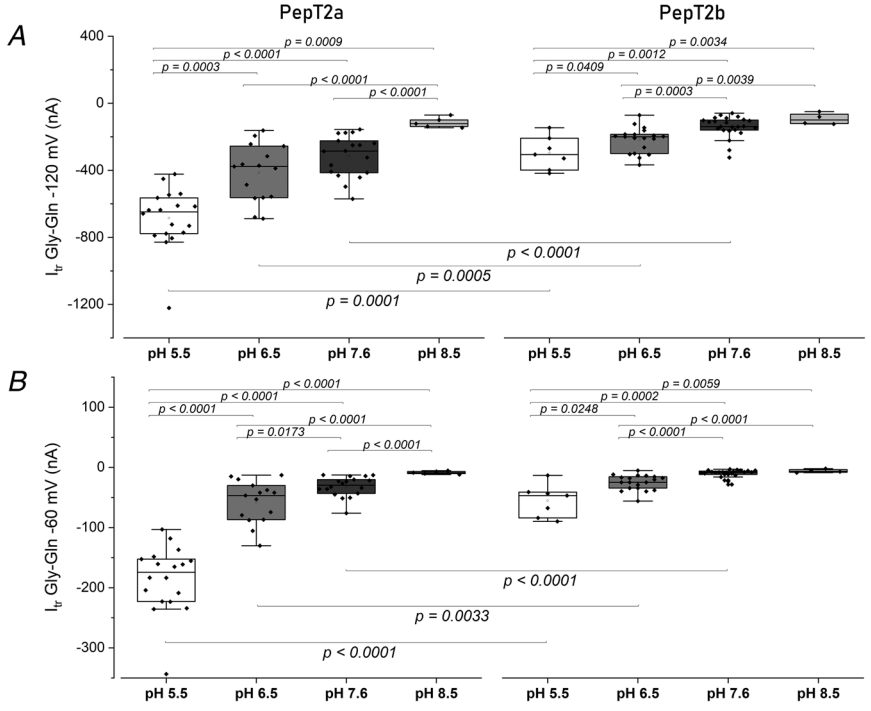

Figure 6. Box plots of the transport current values recorded as reported in Fig. 5, for PepT2a (left) and PepT2b (right) at −120 mV (*A*) and at −60 mV (*B*)
Dots indicate the single oocyte transport current value. In the top part of each figure the statistical comparison between different pH conditions for each transporter is shown. In the bottom, the statistical comparison between transporters at the same pH (two-sample *t* test or Mann-Whitney's U test; $^{*}P < 0.05$, $^{**}P < 0.01$ and $^{***}P < 0.001$) is shown. Samples for box plots are the same as for Fig. 5. The detailed statistical values are reported in the statistical summary document.

Table 3. Kinetic parameters of the transport currents elicited by Gly-Gln in *Xenopus* oocytes. $K_{0.5}$, I_{max} and $I_{max}/K_{0.5}$ values are from Fig. 8. These values were obtained from current/concentration relationship (means (SD)) plotted in Fig. 7, for each voltage and calculated by least-square fit to the Michaelis–Menten eqn (1) and expressed as means (SE) as results of Origin fitting. $I_{max}/K_{0.5}$ is the transport efficiency

		−60 mV			−120 mV			
pH	Neutral form (%)	$K_{0.5}$ (μmol l^{-1})	I_{max} (nA)	$I_{max}/K_{0.5}$ (nA/mmol l^{-1})	$K_{0.5}$ (μmol l^{-1})	I_{max} (nA)	$I_{max}/K_{0.5}$ (nA/mmol l^{-1})	Oocyte/ animals (n/An)
PepT2a								
5.5	99.6	36.9 (9.2)	−192.8 (0.8)	5.2	131.5 (19.6)	−756.8 (61.8)	5.7	13/3
6.5	98.4	25.8 (5.6)	−76.7 (7.2)	3.00	112.6 (24.3)	−543.5 (70.1)	4.8	10/2
7.6	83.0	45.9 (5.2)	−39.5 (2.3)	0.9	107.7 (10.4)	−392.2 (19.3)	3.6	13/3
PepT2b								
5.5	99.6	7.9 (1.2)	−69.2 (4.0)	8.8	35.1 (5.4)	−370.8 (27.6)	10.5	19/3
6.5	98.4	6.6 (1.4)	−25.2 (1.9)	3.8	32.7 (3.3)	−276.3 (15.7)	8.5	16/3
7.6	83.0	24.4 (1.9)	−14.1 (0.5)	0.6	49.6 (21.8)	−241.7 (75.6)	4.9	17/3

−60 mV, $K_{0.5}$ is in the range of tens of micromoles per litre for all the pH for both transporters. However, PepT2b has higher affinity in all the conditions tested for Gly-Gln than PepT2a.

As for most solute carriers, the larger impact on the substrate apparent affinity is due to the hyperpolarization of the membrane voltage that increases the driving force and supports the entrance of substrate and H^+. The efficiency of the transport reflects the two parameters, and it is maximal, as expected, at pH 5.5 in most hyperpolarizing conditions (Fig. 8*C* and *F*). Due to the higher affinity of PepT2b, the efficiency is slightly higher in this transporter and the best working condition is at −120 mV at pH 5.5.

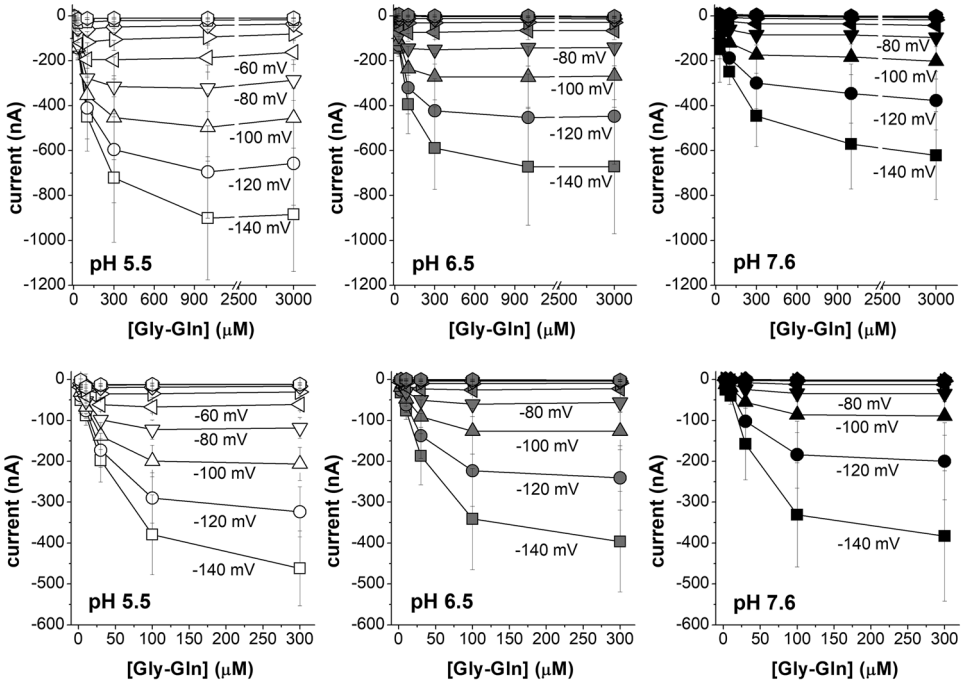

Figure 7. Current *vs*. substrate concentration (*I*/*S*) relationships at the indicated voltages for Atlantic salmon PepT2a in *A*, *B* and *C*, and for PepT2b in *D*, *E* and *F*
The mean value of the currents at each concentration (from 3 μmol l^{-1} to 3 mmol l^{-1} for PepT2a and from 3 μmol l^{-1} to 300 μmol l^{-1} for PepT2b) are plotted at the indicated voltage and pH. Data are means (SD) from 10–19 oocytes, obtained from 2–3 batches. The full series of the mean values (SD) for each concentration, voltage and pH are reported in the statistical summary document. The raw data are available at the link given in the data availability statement.

For the experiment at pH 7.6, for both PepT2-type proteins the currents recorded at membrane voltages higher than −60 mV were too low, and the $K_{0.5}$ or I_{max} obtained were not reliable and, thus, not considered in the analysis.

Presteady-state currents

When a rectangular voltage jump (pulses from −140 to +20 mV in 20 mV increments) protocol is applied to oocytes expressing a transporter, the elicited currents in the absence and presence of the substrate can be a tool for biophysical investigations on the steps of the transport cycle.

Slow transient currents, related to the presence of the transporter in the plasma membrane, were only observed in oocytes expressing the two PepT2-type proteins, and almost completely abolished by the addition of saturating Gly-Gln (1 and 0.3 mmol l^{-1} for PepT2a and PepT2b, respectively) (Fig. 9).

The behaviour of the currents reported in Fig. 9 shows that the pH of the bathing solution affected the current kinetics in both transporters. At pH 5.5, in the absence of substrate, slow transient currents are mostly present in response to depolarizing pulses while at pH 7.6 they are principally present in response to hyperpolarizing pulses; at pH 6.5, the transient currents are symmetrically arranged around the holding potential and are similar for amplitude and decay time (Fig. 9 and Fig. 10*A* and *C*) for hyperpolarizing and depolarizing voltages. This behaviour is more pronounced in PepT2a, where the symmetry at pH 6.5 is almost perfect around the holding voltages.

To study the I_{PSS} component elicited by the voltage jumps, from the traces reported in Fig. 9 the I_{PSS} were separated from the capacitive current of the oocytes as described in *Materials and methods* (see double-exponential function, eqn (2)), assuming that the slow component represents the I_{PSS} (Sangaletti et al., 2009). The currents were then analysed to obtain the biophysical parameters of the transport.

The decay time constant τ and the area underneath the I_{PSS} currents, which correspond to the amounts of charges Q moved in the membrane electric field (Bossi et al., 2011; Peres, Giovannardi et al., 2004; Renna, Sangaletti et al., 2011) were measured at each potential. The τ/V and Q/V obtained at each pH are reported in Fig. 10. Like other peptide transporters, such as mammalian and fish PepT1 (Renna, Oyadeyi et al., 2011; Vacca et al., 2019) and rat PepT2 (Chen et al., 1999), the τ/V curves of both PepT2 appeared bell-shaped (Fig. 10*A* and *C*). Data on τ_{max} at different pH for the two transporters are reported in Table 4.

To better appreciate the pH effect on Q/V curves, the mean values of $Q_{on\text{-}off}$ fitted with the Boltzmann eqn (3) and normalized against the maximal moved charge (Q_{max}) setting the unitary charge level to the saturation value at positive potential (Forlani et al., 2001) are reported in Fig. 10*B* and *D*.

In both transporters, the sigmoidal shape of the charge *vs*. voltage curves showed a clear pH dependence with an inflexion point (Fig. 10*B* and *D*), corresponding to the half of the charge translocation ($Q_{max}/2$), shifted to more negative values of membrane potential ($V_{0.5}$ values in Table 4) as pH increased from 5.5 to 7.6. At pH 7.6 and in depolarization condition (from −20 mV to +20 mV) the

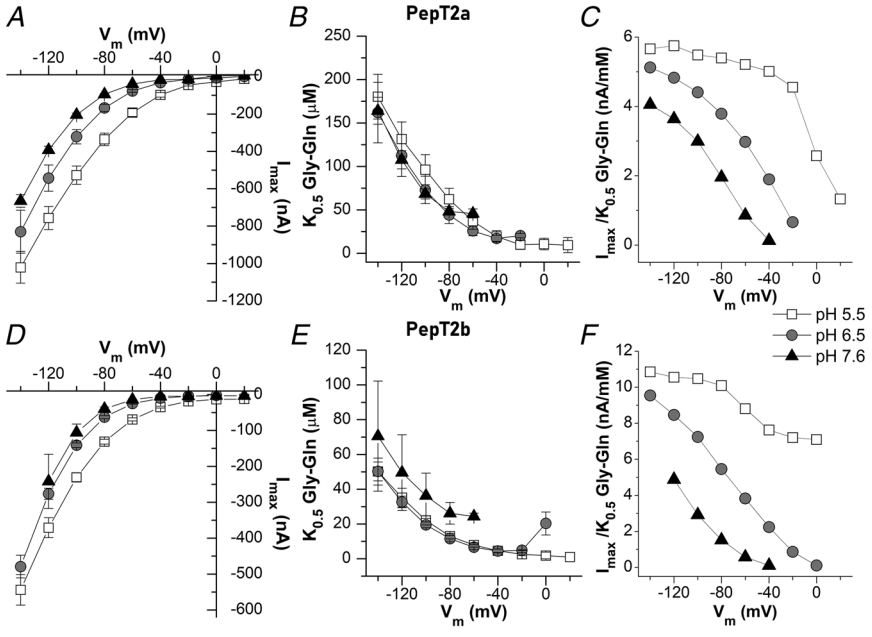

Figure 8. Dose–response analysis: I_{max}, $K_{0.5}$ and transport efficiency of Atlantic salmon PepT2a in *A*, *B* and *C*, and PepT2b in *D*, *E* and *F*
The current values evaluated in the presence of increasing concentrations of Gly-Gln under each tested voltage (reported in Fig. 7 as means (SD)) were subsequently fitted with eqn (1) to obtain the relative maximal current (I_{max}) in *A* and *D*, the $K_{0.5}$ in *B* and *E*, i.e. the substrate concentration that elicits half of the maximal current (I_{max}), and the transport efficiency in *C* and *F*, evaluated as the ratio $I_{max}/K_{0.5}$ under each membrane potential and pH condition. Data are here reported as means (SE) result from Origin fitting. All fit values are reported in the statistical summary document. The raw data are also available at the link indicated in the data availability statement.

Table 4. The maximal value of the decay time constant (τ_{max}) and Boltzmann equation parameters of Atlantic salmon PepT2 proteins (PepT2a and PepT2b) calculated at pH 5.5, 6.5 and 7.6. Q_{hyp} and Q_{dep} represent the amount of displaced charge at hyperpolarizing and depolarizing limits, Q_{max} (= Q_{dep} − Q_{hyp}) is the maximal moveable charge, $V_{0.5}$ is the voltage at which half of the charge is moved, σ represents a slope factor of the sigmoidal curve (Renna, Sangaletti et al., 2011). Parameters were calculated by nonlinear fit to the Boltzmann eqn (3) using Origin 8.0 from the curves of Fig. 10. The number of oocytes for each condition were between 14 and 22, from 2–3 batches

	PepT2a			*PepT2b*		
pH	5.5	6.5	7.6	5.5	6.5	7.6
τ_{max} (ms)	76.8 (6.3)	56.7 (3.6)	48.5 (1.7)	86.9 (3.1)	63.4 (2.3)	46.5 (3.1)
Q_{hyp}(nC)	−2.8 (0.1)	−7.35 (0.05)	−11.8 (0.1)	−9.2 (0.4)	−14.0 (0.2)	−17.5 (0.4)
Q_{dep}(nC)	13.2 (1.2)	6.80 (0.05)	2.20 (0.03)	7.1 (0.2)	4.5 (0.6)	1.21 (0.03)
Q_{max}(nC)	16.1 (1.3)	14.2 (0.1)	14.0 (0.2)	16.3 (0.6)	18.5 (0.3)	18.8 (0.5)
$V_{0.5}$(mV)	4.85 (5.9)	−62.1 (0.3)	−97.6 (0.5)	−70.7 (1.5)	−93.0 (0.7)	−120.5 (1.2)
σ (mV)	42.1 (2.6)	25.1 (0.3)	22.5 (0.4)	42.9 (1.7)	29.2 (0.6)	22.4 (0.5)

Q/V curves showed that PepT2 transporters reached the saturation of the amount of displaced charge. Conversely, charge saturation at negative potential is reached only by PepT2a, at pH 5.5, and in this case, at +20 mV the amount of moved charge is only close to half Q_{max} quite far from the predicted saturation value at depolarizing value (Fig. 10*B*). PepT2b at pH 5.5 presents only the central part of the sigmoid curves, a condition that agrees with the shape of the τ/V curves (Fig. 10*D*).

According to the two-state system representation of the charge movement process (see cartoon in Fig. 11), the parameters obtained by fitting of charge *vs*. voltage curves (Q/V) with the Boltzmann function (Q_{in} and Q_{max}) and the time decay constant *vs*. voltage curves (τ/V) can be used to determine the unidirectional inward and outward rate constants of the charge movement (Renna, Sangaletti et al., 2011).

The charge movement process can be described with a simple reaction where the outrate and the inrate are the unidirectional rate constants:

$$inrate = \frac{1}{\tau}\frac{Q_{in}}{Q_{max}};\ outrate = \frac{1}{\tau}\left(1 - \frac{Q_{in}}{Q_{max}}\right)$$

Q_{in} is the amount of charge located near the inner side of the membrane electrical field and Q_{out} is the amount of charge displaced toward the outer membrane margin.

In Fig. 11, the voltage and pH dependence of the unidirectional rate constants for Atlantic salmon PepT2a and PepT2b transporters are reported. Assuming a positive mobile charge, the outward rates increase when the inner side of the cellular membrane presents a positive voltage and decreases to zero for membrane

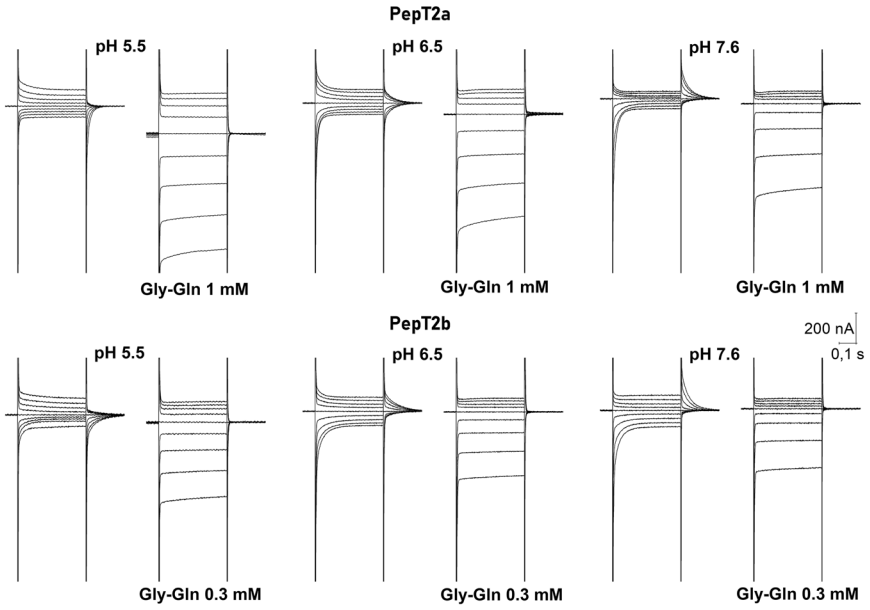

Figure 9. Representative traces of currents elicited by voltage steps protocol applied to *Xenopus* oocytes expressing the Atlantic salmon PepT2 transporters, PepT2a (top) and PepT2b (bottom)
The voltage pulses were in the range −140 to +20 mV. At all tested pH, the presence of saturating concentrations of Gly-Gln (1 mmol l^{-1} for PepT2a and 0.3 mmol l^{-1} for PepT2b) eliminates the transporter transient component (I_{PSS}) and produces large inwardly directed steady-state currents that raise increasing the proton chemical gradient and in hyperpolarization.

voltage values lower than −100/-140 mV. Conversely, the inward rates increase and decrease, respectively, with hyperpolarization and depolarization of the membrane potential.

Within the voltage range tested, both the inward and outward rates of PepT2 proteins showed a variation in the voltage dependence correlated to pH. The inward rates in PepT2a are more affected by voltage than the outward rates (Fig. 11) and a great effect is visible in PepT2a at pH 5.5. Little or no change appears to occur for the inward rate for PepT2b (Fig. 11*D*, *E*). The outward rate instead was more influenced by the voltage at pH 7.6 in PepT2b.

Discussion

In this study, two *slc15a2* genes, named *slc15a2a* and *slc15a2b*, were examined in the Atlantic salmon. Comparison of sequence, structure and gene environment strongly suggests that these two high-affinity/low-capacity transporters have evolved from the WGD event that salmonids experienced 94 million years ago (Lien et al., 2016; Macqueen & Johnston, 2014), where many of the duplicated genes were retained as functional copies. This finding is corroborated by the parallel observation that all other teleost species analysed in this study have only one *slc15a2* gene, with the exception of the salmonids and the goldfish (*Carassium auratum*) a cyprinid the genome of which has also undergone an additional WGD event (Kuang et al., 2016) and also exhibits two *slc15a2* genes. Of note, two genes encoding for PepT2-type transporters, namely *slc15a2a-1* and *slc15a2-2* have been recently described in another cyprinid, the common carp (*Cyprinus carpio*) (Dong et al., 2020). In the Atlantic salmon, genes originating from the salmonid-specific WGD have often been shown to take on new functions (neo-functionalization) or sub-functions (sub-functionalization) of their duplicates (Lien et al., 2016). It is very likely that sub-functionalization has occurred for the Atlantic salmon *slc15a2a* and *slc15a2b*, too. In fact: (i) the Atlantic salmon PepT2a and PepT2b transporters, generated by *slc15a2a* and *slc15a2b*, respectively, are conserved, sharing 87% identity at the amino acid level, and exhibiting all the essential PepT2-type functional motifs; (ii) based on the gene expression data, after the gene duplication event functional divergence may have occurred, and the two identified genes, *slc15a2a* and *slc15a2b*, may have acquired some tissue-specific functions. In this respect, the expression of *slc15a2b*, particularly the very high levels observed in the Atlantic salmon kidney (see Fig. 4*A*), is consistent with the well-known primary function of PepT2 in reabsorbing di/tripeptides from the ultrafiltrate (see, e.g. Boll et al., 1996; Romano et al., 2006; Rubio-Aliaga et al., 2000). Moreover, as previously reported in a variety of teleost fish species (summarized in Table 1), the mRNA expression of *slc15a2b* in the gastrointestinal tract of the Atlantic salmon is mainly confined to the mid-to-distal intestine, a pattern that has been previously observed in the same species (Del Vecchio et al., 2021) and also found in, e.g. the rabbit alimentary canal (Döring et al., 1998). The presence of *slc15a2b* in the distal area of the intestine is most probably related to the enterocytes that secure absorption of small peptides, although the fact that a PepT2-type transporter is also expressed by neurons of the enteric nervous system (Rühl et al., 2005) cannot be ruled out *a priori*. In contrast, in the Atlantic salmon, the *slc15a2a* paralogue exhibits a widespread tissue distribution, in terms of the presence of mRNA, but it is most abundant in the brain and, notably, in the gills. The expression of a PepT2 in the brain, operating as a di/tripeptide uptake system, has been observed in mammals (Biegel et al., 2006; Kamal et al., 2008; Keep & Smith, 2011; Smith et al., 2013; Viennois et al., 2018; Wada et al., 2005) as well

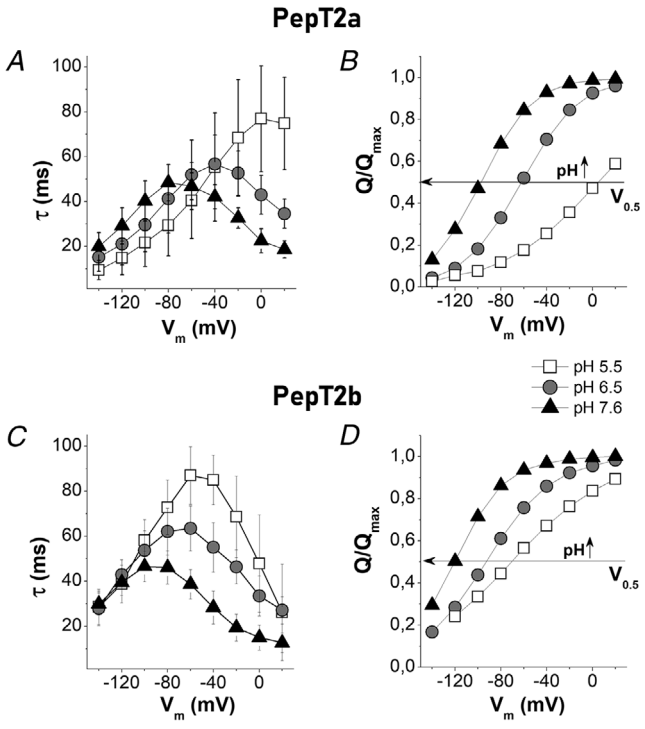

Figure 10. The time constant of decay (τ) and normalized displaced charge (Q/Q_{max}) for Atlantic salmon PepT2 transporters
PepT2a in *A* and *B* and PepT2b in *C* and *D*. τ/V in *A* and *C* and $(Q/Q_{max})/V$ in *B* and *D*. The sample sizes for τ/V and Q/V for each condition were between 14 and 22 oocytes, from 2–3 batches. The τ/V values are the means (SD). The Q/V values are the means normalized against the maximal moveable charge Q_{max} values obtained by fitting using eqn (3). The unitary charge level was set to the saturation value at positive potential. In *B* and *D*, the horizontal arrow intersects each curve at half completion of charge movement corresponding to $V_{0.5}$ given by the Boltzmann eqn (3).

as in teleost fish species, e.g. zebrafish (Romano et al., 2006) and Mozambique tilapia (Con et al., 2019). But, it is noteworthy that the identification of PepT2 mRNA transcripts in the gills leads to the hypothesis that a di/tripeptide transporter might also be operating in such an epithelial tissue, moving di/tripeptides directly from the aquatic environment to the blood and/or vice versa.

The fact that key amino acids involved in substrate recognition and transport are well conserved between Atlantic salmon and mammalian (rat and human) PepT2 proteins (Fig. 1*A*), and that both salmon PepT2a and PepT2b protein structures share about 55% identity with the mammalian homologue (Fig. 1*B*), indicates that their function is conserved across species. Indeed, both PepT2a and PepT2b in the presence of dipeptides (Gly-Gln) elicit inward currents, as it does for the other *Slc15* members (Biegel et al., 2006; Chen et al., 1999; Romano et al., 2006; Rubio-Aliaga et al., 2000; Saito et al., 1996; Terada et al., 2000; Verri et al., 2017). These currents are pH-dependent and Na^+-independent, with inward coupled currents being recorded even when Gly-Gln is perfused at pH 8.5. However, the transport current is three times higher in PepT2a than PepT2b and at pH 5.5 the current rapidly decreases after the first seconds of substrate perfusion (Fig. 5). This phenomenon is not new in solute carriers (Eskandari et al., 1997; Mackenzie et al., 1996; Mackenzie et al., 1998) or in PepT2 transporters (Chen et al., 1999). It is observed in cotransporters expressed in oocytes, mainly at substrate concentrations above the apparent $K_{0.5}$. The decreases in current after the peak can be due to decreased H^+ concentrations at the immediate proximity of the extracellular membrane or to the increase of intracellular substrate or H^+ accumulation, analogous to explanations for PepT1 (Bossi et al., 2011; Kottra & Daniel, 2001; Kottra et al., 2002; Kottra et al., 2009) and PepT2 (Chen et al., 1999). For PepT2b, however, a different behaviour is observed. In this transporter, the removal of 1 mmol l^{-1} Gly-Gln at the end of the perfusion time induces a rapid and fast increasing current at pH 5.5, suggesting that substrate concentration at 1 mmol l^{-1}, which is a concentration higher than the saturating value of 300 μM, reduced the final transport current. The behaviour is related to the accumulation of substrate inside the cell and to the high affinity of the transporter for the substrate. In this case, the net flux at very high substrate concentration results lower than the flux at the concentration proximal to saturation value (Bosdriesz et al., 2018; Mertl et al., 2008; Renna, Oyadeyi et al., 2011).

Dose–current experiments at different pH and voltage confirm that the two Atlantic salmon PepT2 proteins behave as high-affinity/low-capacity transporters. The

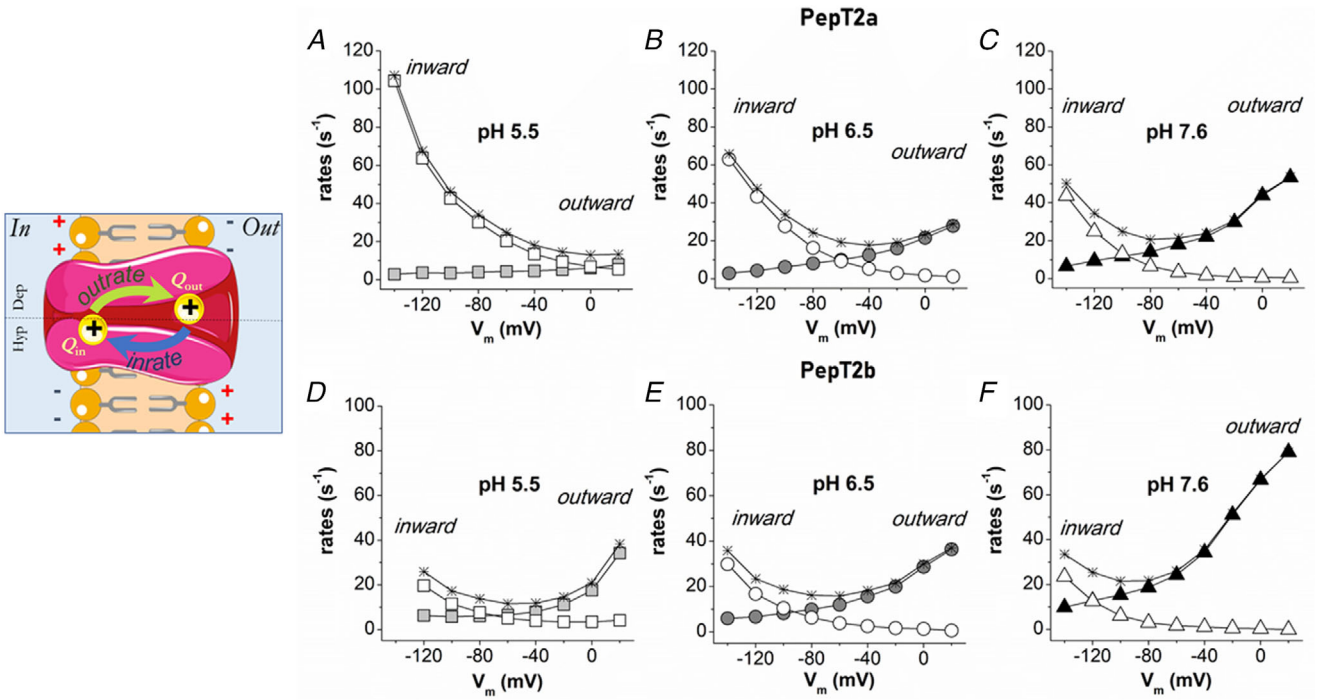

Figure 11. The unidirectional rate constants
Graphical representation of a two-state system (left). Inward (open symbols) and outward (solid symbols) rate constants of the intramembrane charge movement of Atlantic salmon PepT2 transporters, PepT2a in *A*, *B* and *C*, and PepT2b in *D*, *E* and *F*. The unidirectional rates, plotted as a function of membrane potentials, were calculated from τ/V (and $(Q/Q_{max})/V$ (in Fig. 10) at the different pH. The rate ($1/\tau$) of the two transporters are plotted as stars. [Colour figure can be viewed at wileyonlinelibrary.com]

'canonical' renal transporter PepT2b shows a higher affinity and smaller current if compared with the 'brain/gills' PepT2a. When the apparent affinity ($1/K_{0.5}$) and I_{max} are determined and plotted *vs.* voltage at different pH, other functional characteristics distinguish the two Atlantic salmon proteins. Atlantic salmon PepT2a and PepT2b tested in the same conditions, using the same protocol and substrate, have specific transport characteristics which are underlined by the detailed biophysical and kinetic analysis presented in Fig. 8. The data on the PepT2b transporter are very similar to the data collected for the zebrafish (Romano et al., 2006) and recall the rabbit PepT2 (Amasheh et al., 1997), but with less marked pH differences. In fact, in Atlantic salmon PepT2b, the reduction of H^+ is balanced by the hyperpolarizing voltages (see comment in Sala-Rabanal et al., 2008). Many solute carriers have charged residues located in the transmembrane helices. When the membrane voltage is rapidly changed across the membrane (voltage jumps) some charges of these residues turn to new equilibrium positions, giving rise to I_{PSS} (Lester et al., 1996; Loo et al., 1998; Mager et al., 1996; Peres, Pisani et al., 2004). These I_{PSS} disappear when the new equilibrium is achieved. Furthermore, binding or unbinding of substrate or more often of the driving ions is voltage dependent and can contribute to the generation of the I_{PSS} (Bossi et al., 2002; Bossi et al., 2012; Cherubino et al., 2012; Fesce et al., 2002). In this respect, I_{PSS} analyses provide a unique opportunity to collect information on the kinetic properties and the transport cycle of the Atlantic salmon PepT2 transporters. In contrast to PepT1 transporters, which have been thoroughly characterized in both mammals and teleosts (Mackenzie et al., 1996; Nussberger et al., 1997; Renna, Sangaletti et al., 2011; Sangaletti et al., 2009), data on I_{PSS} of PepT2 are lacking. Only two papers (Chen et al., 1999; Sala-Rabanal et al., 2008) analysed a few conditions, limited to rat and human transporters, and information about the relationship between charge movements and transport processes in PepT2 is otherwise completely missing for other species and fish. As previously described for oocytes expressing the rat (Chen et al., 1999) and human (Sala-Rabanal et al., 2008) PepT2, Atlantic salmon PepT2a- and PepT2b-injected oocytes show transient currents after step changes in membrane potential. Unlike most transporters in which I_{PSS} have been analysed, in mammalian PepT2 two peculiar effects were reported. First, both Chen et al. (1999) and Sala-Rabanal et al. (2008) report that the presence of I_{PSS} is increased at acidic pH in the presence of substrate, of non-saturating concentrations (lower than $K_{0.5}$) for human transporter, and saturating concentrations for the rat transporter. Furthermore, for the human transporter a discrepancy of the Q_{on} and Q_{off} has also been observed, according to the length of the interval between the voltage steps (time that is necessary to revert to the inactivated state). Instead, the behaviour of both salmon PepT2 I_{PSS} and the relative parameter is similar to the 'classical' model and to that reported for PepT1. The I_{PSS} were larger in the absence of substrate at all pH tested and Q_{on} and Q_{off} were always similar. The effect of varying the external H^+ concentration on PepT2 I_{PSS} kinetics is emphasized by the shift toward more negative potentials of both the maximal time constant (τ_{max}) and the half of the moved maximal charge ($Q_{max}/2$), in response to increasing pH of the external medium. Accordingly, the same effect of the pH is observed on the shift of the crossing point between the inward and outward rates. In Atlantic salmon PepT2a, the saturation of the amount of displaced charge at more hyperpolarizing potentials at pH 5.5 is coherent with the high acceleration of the inward rate. Conversely, for both Atlantic salmon PepT2, at pH 7.6 the saturation of the moved charge at depolarizing potentials is reached and is associated with an acceleration of the outward rate. This effect is more evident in Atlantic salmon PepT2b, in agreement with the data reported in Fig. 11. Together, these data confirm that for the two Atlantic salmon PepT2 transporters the polarity of I_{PSS} kinetics and the magnitude of the charge movements are strictly dependent on the H^+ electrochemical potential across the plasma membrane (Mager et al., 1998).

The comparison between the $V_{0.5}$ values of PepT2a and PepT2b reveals marked differences at the same pH with $V_{0.5}$ of Atlantic salmon PepT2a right-shifted (Table 4). The slope factor (σ) is instead similar at each pH showing that the two PepT2 transporters exhibit a similar fraction of the electrical field where the charge movement occurs. It is also important to highlight that the Q_{max} showed similar values in all the conditions (Table 4). Considering that the I_{PSS} are mainly due to intrinsic charges of the protein that are moveable, the fact that Q_{max} does not change in the tested conditions suggests that the expression on the membrane of the *Xenopus* oocytes of the two transporters is similar (Forster et al., 2006; Mager et al., 1993). To summarize, our experimental data suggest that for both Atlantic salmon PepT2 transporters (i) the maximal charge displacement (Q_{max}) is independent of external proton concentration (Table 4); (ii) the charge movement in the on-response (Q_{on}) is balanced by the charge moved in the off transition (Q_{off}) at all potential jumps from the holding voltage; (iii) the addition of substrate at saturating concentration eliminates the I_{PSS} for all tested pH conditions and produces large inwardly directed steady-state transport currents; and (iv) acidification causes a positive shift in the voltage dependence of both presteady-state and steady-state related parameters. Based on all four observations listed above, qualitatively kinetic models can be hypothesized, in which in the empty transporters negatively charged and protonated, 'trapping' states are introduced to account for the voltage shift

produced by pH. Indeed, the kinetic schemes proposed by Sala-Rabanal et al. (2008) and Chen et al. (1999) can qualitatively account for the effect of the pH on the unidirectional rate constant shown in Fig. 11 and consequently of the τ/V and Q/V curves of Fig. 10. A scheme of the kinetic state is shown in Fig. 12 and include a voltage-independent and fast binding of a second proton (transition II→III in Fig. 12). As detailed in Mager et al. (1998) for the neurotransmitter transporter GAT1, sequential binding of a second driving ion would reduce the outward rate constant of charge movement, an effect observed in GAT1 with Na^+ ions and in both PepT2a and PepT2b with H^+. This effect is much more significant in rat and human PepT2 transporters where it conducts to the inactive state at acidic pH. Conversely, the transition I←II represented in Fig. 12 dependent on external protons will speed up the inward rate, particularly for PepT2a, again in agreement with the rate constant (Fig. 11*A*).

The different behaviour at acidic pH between piscine and mammalian transporters could be related to the potency of the 'trapped- state' (Chen et al., 1999; Sala-Rabanal et al., 2008) that is hypothesized to involve the binding competition between protons and substrates. In the mammalian transporters, hyperpolarization at acidic pH appears to have inactivating effects on I_{PSS} and steady-state properties, as in human and rat PepT2 the substrate-evoked current and substrate affinity decrease at very negative voltages at pH 5.5. In Atlantic salmon transporters, substrate affinity at hyperpolarizing potential decreases but it is not affected by pH; in the range of voltages tested, the steady-state currents are not reduced by acidification and the I_{PSS} is recorded in the absence of the substrate and disappears in its presence. On the contrary, in the mammalian PepT2 the presence of external substrate seems to have a role in reducing the transporter inactivation by hyperpolarization because it increases the I_{PSS} and the maximal steady-state currents (I_{max}) evoked by saturating substrate concentrations. The biophysical characterization of piscine PepT2 transporters and the data reported about the I_{PSS} could be the foundation for future investigations on the relationship between proton and substrate in the translocation steps of the peptide transporter family. In particular, it is of great interest that in all the PepT-type transporters functionally characterized so far, the residues identified by the recent structural model (Killer et al., 2021; Parker et al., 2021) as involved in the transporter activity, are conserved (Fig. 1). In light of the results reported here, it will be essential to investigate residues that are not the main actors in transport activity but that could be responsible for the subtle changes in proton and substrate affinity, changes in substrate selectivity (Margheritis et al., 2013; Pieri et al., 2009; Xu et al., 2010) and to model their role in a specific transporter of interest.

Conclusions

The Atlantic salmon is the second teleost fish species (Gomes et al., 2020; Ronnestad et al., 2010) (this paper), after the zebrafish (Romano et al., 2006; Vacca et al., 2019; Verri et al., 2003), for which both PepT1- and PepT2-type transporters have been functionally characterized. Due to a salmonid-specific WGD, two functional PepT2-type transporters operate in the Atlantic salmon which seems to have resulted in a split of functions with respect to the canonical situation described in mammals, in which a single PepT2 transporter operates in the whole organism. In this respect, our description of the Atlantic salmon,

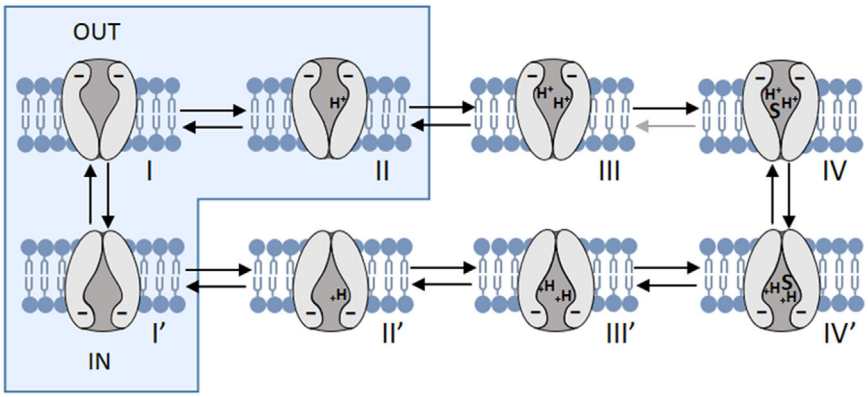

Figure 12. Representation of two kinetic models for PepT2 transporter
Each configuration represents a state, from I to IV (outside) and from I' to IV' (inside). The presteady-state currents arise from the redistribution of the negatively charged transporter between states I', I and II (blue boxes). The binding of the first external proton to state I accelerates the inward rate constant, while the binding of a second proton to state II leads to state III, effectively slowing down the outward rate. Transitions between I', I and II are voltage dependent. S represents the binding of the substrate. Modified from Chen et al. (1999) and Sala-Rabanal et al. (2008). [Colour figure can be viewed at wileyonlinelibrary.com]

where one of the transporters (PepT2b) is expressed in kidney and mid-to-distal intestine, while the other (PepT2a) is expressed in the brain and gills, represents a novel paradigm in the vertebrates. Both transporters have specific transport traits, detailed here by biophysical and kinetic analysis. Moreover, the kinetic schemes previously proposed for two mammalian PepT2 transporters and the recently mechanistic structural models can qualitatively account for the transport structure and function. In a wider perspective, an effort is still needed to complete the local distribution of the two PepT2-type transporters in the various tissues/organs of the Atlantic salmon and demonstrate that these are expressed at the protein level. Also, the analysis of the regulation of these transporters remains open for future studies, as well as if and how they differentially respond to various external stimuli and environmental conditions, such as dietary nutrients, salinity and temperature. Finally, the availability of detailed functional data from distant orthologues of the same protein certainly presents a key tool for investigating how single determinants could be responsible for subtle functional differences (Castagna et al., 2022), as the differences in sequence can easily be related to differences in the kinetic or biophysical parameters. From this point of view, the data here reported will surely help in the investigation on the structure–function relationships within the peptide transporter family.

References

Ahmed, M., Liang, H., Chisomo Kasiya, H., Ji, K., Ge, X., Ren, M., Liu, B., Zhu, X., & Sun, A. (2019). Complete replacement of fish meal by plant protein ingredients with dietary essential amino acids supplementation for juvenile blunt snout bream (Megalobrama amblycephala). *Aquaculture Nutrition*, **25**, 205–214.

Amasheh, S., Wenzel, U., Weber, W. M., Clauss, W., & Daniel, H. (1997). Electrophysiological analysis of the function of the mammalian renal peptide transporter expressed in Xenopus laevis oocytes. *Journal of Physiology*, **504**(Pt 1), 169–174.

Barat, A., Sahoo, P. K., Kumar, R., & Pande, V. (2016). Solute carriers (SLCs) identified and characterized from kidney transcriptome of golden mahseer (Tor putitora) (Fam: Cyprinidae). *Comparative Biochemistry and Physiology Part B, Biochemistry & Molecular Biology*, **200**, 54–61.

Biegel, A., Knütter, I., Hartrodt, B., Gebauer, S., Theis, S., Luckner, P., Kottra, G., Rastetter, M., Zebisch, K., Thondorf, I., Daniel, H., Neubert, K., & Brandsch, M. (2006). The renal type H+/peptide symporter PEPT2: Structure-affinity relationships. *Amino Acids*, **31**, 137–156.

Boll, M., Herget, M., Wagener, M., Weber, W. M., Markovich, D., Biber, J., Clauss, W., Murer, H., & Daniel, H. (1996). Expression cloning and functional characterization of the kidney cortex high-affinity proton-coupled peptide transporter. *Proceedings National Academy of Science USA*, **93**, 284–289.

Bosdriesz, E., Wortel, M. T., Haanstra, J. R., Wagner, M. J., de laTorre Cortés, P., & Teusink, B. (2018). Low affinity uniporter carrier proteins can increase net substrate uptake rate by reducing efflux. *Scientific Reports*, **8**, 5576.

Bossi, E., Cherubino, F., Margheritis, E., Oyadeyi, A. S., Vollero, A., & Peres, A. (2012). Temperature effects on the kinetic properties of the rabbit intestinal oligopeptide cotransporter PepT1. *Pflugers Archiv: European journal of Physiology*, **464**, 183–191.

Bossi, E., Fabbrini, M. S., & Ceriotti, A. (2007). Exogenous protein expression in Xenopus Laevis Oocyte, Basic procedure. In G.Grandi (ed.), *Vitro transcription and translation protocols*, (375 edn, pp. 107–131). Humana Press, Totowa NJ.

Bossi, E., Giovannardi, S., Binda, F., Forlani, G., & Peres, A. (2002). Role of anion-cation interactions on the pre-steady-state currents of the rat Na(+)-Cl(-)-dependent GABA cotransporter rGAT1. *Journal of Physiology*, **541**, 343–350.

Bossi, E., Renna, M. D., Sangaletti, R., D'Antoni, F., Cherubino, F., Kottra, G., & Peres, A. (2011). Residues R282 and D341 act as electrostatic gates in the proton-dependent oligopeptide transporter PepT1. *Journal of Physiology*, **589**, 495–510.

Buracco, S., Peracino, B., Cinquetti, R., Signoretto, E., Vollero, A., Imperiali, F., Castagna, M., Bossi, E., & Bozzaro, S. (2015). Dictyostelium Nramp1, which is structurally and functionally similar to mammalian DMT1 transporter, mediates phagosomal iron efflux. *Journal of Cell Science*, **128**, 3304–3316.

Castagna, M., Cinquetti, R., Verri, T., Vacca, F., Giovanola, M., Barca, A., Romanazzi, T., Roseti, C., Galli, A., & Bossi, E. (2022). The lepidopteran KAAT1 and CAATCH1: Orthologs to understand structure-function relationships in mammalian SLC6 transporters. *Neurochemical Research*, **47**, 111–126.

Chen, X. Z., Zhu, T., Smith, D. E., & Hediger, M. A. (1999). Stoichiometry and kinetics of the high-affinity H+-coupled peptide transporter PepT2. *Journal of Biological Chemistry*, **274**, 2773–2779.

Cherubino, F., Bertram, S., Bossi, E., & Peres, A. (2012). Pre-steady-state and reverse transport currents in the GABA transporter GAT1. *American Journal of Physiology Cell Physiology*, **302**, C1096-C1108.

Chourasia, T. K., D'Cotta, H., Baroiller, J. F., Slosman, T., & Cnaani, A. (2018). Effects of the acclimation to high salinity on intestinal ion and peptide transporters in two tilapia species that differ in their salinity tolerance. *Comparative Biochemistry and Physiology Part A, Molecular & Integrative Physiology*, **218**, 16–23.

Con, P., Nitzan, T., & Cnaani, A. (2017). Salinity-dependent shift in the localization of three peptide transporters along the intestine of the mozambique tilapia (Oreochromis mossambicus). *Frontiers in Physiology*, **8**, 8.

Con, P., Nitzan, T., Slosman, T., & Cnaani, A. (2021). Water salinity and postprandial effects on transcription of peptide and amino acid transporters in the kidney of Mozambique tilapia (Oreochromis mossambicus). *Aquaculture*, **536**, 736384.

Con, P., Nitzan, T., Slosman, T., Harpaz, S., & Cnaani, A. (2019). Peptide transporters in the primary gastrointestinal tract of pre-feeding mozambique tilapia larva. *Frontiers in Physiology*, **10**, 808.

deCastro, E., Sigrist, C. J., Gattiker, A., Bulliard, V., Langendijk-Genevaux, P. S., Gasteiger, E., Bairoch, A., & Hulo, N. (2006). ScanProsite: detection of PROSITE signature matches and ProRule-associated functional and structural residues in proteins. *Nucleic Acids Research*, **34**, W362-W365.

Delpire, E., Gagnon, K. B., Ledford, J. J., & Wallace, J. M. (2011). Housing and husbandry of Xenopus laevis affect the quality of oocytes for heterologous expression studies. *Journal of the American Association for Laboratory Animal Science : JAALAS*, **50**, 46–53.

Del Vecchio, G., Lai, F., Gomes, A. S., Verri, T., Kalananthan, T., Barca, A., Handeland, S., & Rønnestad, I. (2021). Effects of short-term fasting on mRNA expression of ghrelin and the peptide transporters PepT1 and 2 in atlantic salmon (Salmo salar). *Frontiers in Physiology*, **12**, 666670.

Dong, C., Jiang, Z., Zhang, X., Feng, J., Wang, L., Tian, X., Xu, P., & Li, X. (2020). Phylogeny of Slc15 family and response to Aeromonas hydrophila infection following Lactococcus lactis dietary supplementation in Cyprinus carpio. *Fish & Shellfish Immunology*, **106**, 705–714.

Döring, F., Walter, J., Will, J., Föcking, M., Boll, M., Amasheh, S., Clauss, W., & Daniel, H. (1998). Delta-aminolevulinic acid transport by intestinal and renal peptide transporters and its physiological and clinical implications. *The Journal of Clinical Investigation*, **101**, 2761–2767.

Eskandari, S., Loo, D. D., Dai, G., Levy, O., Wright, E. M., & Carrasco, N. (1997). Thyroid Na+/I- symporter. Mechanism, stoichiometry, and specificity. *Journal of Biological Chemistry*, **272**, 27230–27238.

Fesce, R., Giovannardi, S., Binda, F., Bossi, E., & Peres, A. (2002). The relation between charge movement and transport-associated currents in the rat GABA cotransporter rGAT1. *Journal of Physiology*, **545**, 739–750.

Forlani, G., Bossi, E., Ghirardelli, R., Giovannardi, S., Binda, F., Bonadiman, L., Ielmini, L., & Peres, A. (2001). Mutation K448E in the external loop 5 of rat GABA transporter rGAT1 induces pH sensitivity and alters substrate interactions. *Journal of Physiology*, **536**, 479–494.

Forster, I. C., Virkki, L., Bossi, E., Murer, H., & Biber, J. (2006). Electrogenic kinetics of a Mammalian intestinal type IIb na(+)/p (I) cotransporter. *The Journal of Membrane Biology*, **212**, 177–190.

Gomes, A. S., Vacca, F., Cinquetti, R., Murashita, K., Barca, A., Bossi, E., Ronnestad, I., & Verri, T. (2020). Identification and characterization of the Atlantic salmon peptide transporter 1a. *American Journal of Physiology Cell Physiology*, **318**, C191-C204.

Huang, Q., Vera Delgado, J. M., Seni Pinoargote, O. D., & Llaguno, R. A. (2015). Molecular evolution of the Slc15 family and its response to waterborne copper and mercury exposure in tilapia. *Aquatic Toxicology (Amsterdam, Netherlands)*, **163**, 140–147.

Ji, K., He, J., Liang, H., Ren, M., Ge, X., & Masagounder, K. (2021). Response of gibel carp (Carassius auratus gibelio) to increasing levels of dietary lysine in zero fish meal diets. *Aquaculture Nutrition*, **27**, 49–62.

Jones, D. T., Taylor, W. R., & Thornton, J. M. (1992). The rapid generation of mutation data matrices from protein sequences. *Bioinformatics*, **8**, 275–282.

Jumper, J., Evans, R., Pritzel, A., Green, T., Figurnov, M., Ronneberger, O., Tunyasuvunakool, K., Bates, R., Žídek, A., Potapenko, A., Bridgland, A., Meyer, C., Kohl, S. A. A., Ballard, A. J., Cowie, A., Romera-Paredes, B., Nikolov, S., Jain, R., Adler, J., … Hassabis, D. (2021). Highly accurate protein structure prediction with AlphaFold. *Nature*, **596**, 583–589.

Kamal, M. A., Keep, R. F., & Smith, D. E. (2008). Role and relevance of PEPT2 in drug disposition, dynamics, and toxicity. *Drug Metabolism and Pharmacokinetics*, **23**, 236–242.

Keep, R. F., & Smith, D. E. (2011). Choroid plexus transport: Gene deletion studies. *Fluids and Barriers of the CNS*, **8**, 26.

Killer, M., Wald, J., Pieprzyk, J., Marlovits, T. C., & Low, C. (2021). Structural snapshots of human PepT1 and PepT2 reveal mechanistic insights into substrate and drug transport across epithelial membranes. *Science Advances*, **7**, eabk3259.

Kokou, F., Con, P., Barki, A., Nitzan, T., Slosman, T., Mizrahi, I., & Cnaani, A. (2019). Short- and long-term low-salinity acclimation effects on the branchial and intestinal gene expression in the European seabass (Dicentrarchus labrax). *Comparative biochemistry and physiology Part A, Molecular & Integrative Physiology*, **231**, 11–18.

Kottra, G., & Daniel, H. (2001). Bidirectional electrogenic transport of peptides by the proton-coupled carrier PEPT1 in Xenopus laevis oocytes: Its asymmetry and symmetry. *Journal of Physiology*, **536**, 495–503.

Kottra, G., Frey, I., & Daniel, H. (2009). Inhibition of intracellular dipeptide hydrolysis uncovers large outward transport currents of the peptide transporter PEPT1 in Xenopus oocytes. *Pflugers Archiv : European Journal of Physiology*, **457**, 809–820.

Kottra, G., Stamfort, A., & Daniel, H. (2002). PEPT1 as a paradigm for membrane carriers that mediate electrogenic bidirectional transport of anionic, cationic, and neutral substrates. *The Journal of Biological Chemistry*, **277**, 32683–32691.

Kuang, Y.-Y., Zheng, X.-H., Li, C.-Y., Li, X.-M., Cao, D.-C., Tong, G.-X., Lv, W.-H., Xu, W., Zhou, Y., Zhang, X.-F., Sun, Z.-P., Mahboob, S., Al-Ghanim, K. A., Li, J.-T., & Sun, X.-W. (2016). The genetic map of goldfish (Carassius auratus) provided insights to the divergent genome evolutions in the Cyprinidae family. *Scientific Reports*, **6**, 34849.

Kumar, S., Stecher, G., Li, M., Knyaz, C., & Tamura, K. (2018). MEGA X: Molecular evolutionary genetics analysis across computing platforms. *Molecular Biology and Evolution*, **35**, 1547–1549.

Lester, H. A., Cao, Y., & Mager, S. (1996). Listening to neurotransmitter transporters. *Neuron*, **17**, 807–810.

Lien, S., Koop, B. F., Sandve, S. R., Miller, J. R., Kent, M. P., Nome, T., Hvidsten, T. R., Leong, J. S., Minkley, D. R., Zimin, A., Grammes, F., Grove, H., Gjuvsland, A., Walenz, B., Hermansen, R. A., vonSchalburg, K., Rondeau, E. B., Di Genova, A., Samy, J. K. A., … Davidson W. S. (2016). The Atlantic salmon genome provides insights into rediploidization. *Nature*, **533**, 200–205.

Liu, W., Liang, R., Ramamoorthy, S., Fei, Y. J., Ganapathy, M. E., Hediger, M. A., Ganapathy, V., & Leibach, F. H. (1995). Molecular cloning of PEPT 2, a new member of the H+/peptide cotransporter family, from human kidney. *Biochimica Et Biophysica Acta*, **1235**, 461–466.

Loo, D. D., Hirayama, B. A., Gallardo, E. M., Lam, J. T., Turk, E., & Wright, E. M. (1998). Conformational changes couple Na+ and glucose transport. *PNAS*, **95**, 7789–7794.

Mackenzie, B., Loo, D. D., Fei, Y., Liu, W. J., Ganapathy, V., Leibach, F. H., & Wright, E. M. (1996). Mechanisms of the human intestinal H+-coupled oligopeptide transporter hPEPT1. *Journal of Biological Chemistry*, **271**, 5430–5437.

Mackenzie, B., Loo, D. D., & Wright, E. M. (1998). Relationships between Na+/glucose cotransporter (SGLT1) currents and fluxes. *The Journal of Membrane Biology*, **162**, 101–106.

Macqueen, D. J., & Johnston, I. A. (2014). A well-constrained estimate for the timing of the salmonid whole genome duplication reveals major decoupling from species diversification. *Proceedings Biological Sciences*, **281**, 20132881.

Mager, S., Cao, Y., & Lester, H. A. (1998). Measurement of transient currents from neurotransmitter transporters expressed in Xenopus oocytes. *Methods in Enzymology*, **296**, 551–566.

Mager, S., KleinbergerDoron, N., Keshet, G. I., Davidson, N., Kanner, B. I., & Lester, H. A. (1996). Ion binding and permeation at the GABA transporter GAT1. *Journal of Neuroscience*, **16**, 5405–5414.

Mager, S., Naeve, J., Quick, M., Labarca, C., Davidson, N., & Lester, H. A. (1993). Steady states, charge movements, and rates for a cloned GABA transporter expressed in Xenopus oocytes. *Neuron*, **10**, 177–188.

Margheritis, E., Terova, G., Oyadeyi, A. S., Renna, M. D., Cinquetti, R., Peres, A., & Bossi, E. (2013). Characterization of the transport of lysine-containing dipeptides by PepT1 orthologs expressed in Xenopus laevis oocytes. *Comparative Biochemistry and Physiology Part A, Molecular & Integrative Physiology*, **164**, 520–528.

McNamara, S., Wlizla, M., & Horb, M. E. (2018). Husbandry, general care, and transportation of xenopus laevis and xenopus tropicalis. *Methods in Molecular Biology (Clifton, NJ)*, **1865**, 1–17.

Mertl, M., Daniel, H., & Kottra, G. (2008). Substrate-induced changes in the density of peptide transporter PEPT1 expressed in Xenopus oocytes. *AmJPhysiol Cell Physiol*, **295**, C1332-C1343.

Nussberger, S., Steel, A., Trotti, D., Romero, M. F., Boron, W. F., & Hediger, M. A. (1997). Symmetry of H+ binding to the intra- and extracellular side of the H+-coupled oligipeptide cotransporter PepT1. *Journal of Biological Chemistry*, **272**, 7777–7785.

Ostaszewska, T., Dabrowski, K., Kamaszewski, M., Grochowski, P., Verri, T., Rzepkowska, M., & Wolnicki, J. (2010). The effect of plant protein-based diet supplemented with dipeptide or free amino acids on digestive tract morphology and PepT1 and PepT2 expressions in common carp (Cyprinus carpio L.). *Comparative Biochemistry and Physiology Part A, Molecular & Integrative Physiology*, **157**, 158–169.

Parker, J. L., Deme, J. C., Wu, Z., Kuteyi, G., Huo, J., Owens, R. J., Biggin, P. C., Lea, S. M., & Newstead, S. (2021). Cryo-EM structure of PepT2 reveals structural basis for proton-coupled peptide and prodrug transport in mammals. *Science Advances*, **7**, eabh3355.

Peres, A., Giovannardi, S., Bossi, E., & Fesce, R. (2004). Electrophysiological insights into the mechanism of ion-coupled cotransporters. *News in Physiological Sciences*, **19**, 80–84.

Peres, A., Pisani, R., Soragna, A., & Fesce, R. (2004). Biophysical approaches to the study of ion coupled transport protein. *Recent Res Devel Membrane Biol*, **2**, 1–19.

Pieri, M., Gan, C., Bailey, P., & Meredith, D. (2009). The transmembrane tyrosines Y56, Y91 and Y167 play important roles in determining the affinity and transport rate of the rabbit proton-coupled peptide transporter PepT1. *International Journal of Biochemistry & Cell Biology*, **41**, 2204–2213.

Renna, M. D., Oyadeyi, A. S., Bossi, E., Kottra, G., & Peres, A. (2011). Functional and structural determinants of reverse operation in the pH-dependent oligopeptide transporter PepT1. *Cellular and Molecular Life Sciences*, **68**, 2961–2975.

Renna, M. D., Sangaletti, R., Bossi, E., Cherubino, F., Kottra, G., & Peres, A. (2011). Unified modeling of the mammalian and fish proton-dependent oligopeptide transporter PepT1. *Channels (Austin)*, **5**, 89–99.

Romano, A., Barca, A., Storelli, C., & Verri, T. (2014). Teleost fish models in membrane transport research: The PEPT1(SLC15A1) H+-oligopeptide transporter as a case study. *Journal of Physiology*, **592**, 881–897.

Romano, A., Kottra, G., Barca, A., Tiso, N., Maffia, M., Argenton, F., Daniel, H., Storelli, C., & Verri, T. (2006). High-affinity peptide transporter PEPT2 (SLC15A2) of the zebrafish Danio rerio: Functional properties, genomic organization, and expression analysis. *Physiological Genomics*, **24**, 207–217.

Ronnestad, I., Murashita, K., Kottra, G., Jordal, A. E., Narawane, S., Jolly, C., Daniel, H., & Verri, T. (2010). Molecular cloning and functional expression of atlantic salmon peptide transporter 1 in Xenopus oocytes reveals efficient intestinal uptake of lysine-containing and other bioactive di- and tripeptides in teleost fish. *Journal of Nutrition*, **140**, 893–900.

Rubio-Aliaga, I., Boll, M., & Daniel, H. (2000). Cloning and characterization of the gene encoding the mouse peptide transporter PEPT2. *Biochemical and Biophysical Research Communications*, **276**, 734–741.

Ruhl, A., Hoppe, S., Frey, I., Daniel, H., & Schemann, M. (2005). Functional expression of the peptide transporter PEPT2 in the mammalian enteric nervous system. *Journal of Comparative Neurology*, **490**, 1–11.

Saito, H., Terada, T., Okuda, M., Sasaki, S., & Inui, K. (1996). Molecular cloning and tissue distribution of rat peptide transporter PEPT2. *Biochimica Et Biophysica Acta*, **1280**, 173–177.

Sala-Rabanal, M., Loo, D. D., Hirayama, B. A., & Wright, E. M. (2008). Molecular mechanism of dipeptide and drug transport by the human renal H+/oligopeptide cotransporter hPEPT2. *American Journal of Physiology Renal Physiology*, **294**, F1422-F1432.

Sangaletti, R., Terova, G., Peres, A., Bossi, E., Cora, S., & Saroglia, M. (2009). Functional expression of the oligopeptide transporter PepT1 from the sea bass (Dicentrarchus labrax). *Pflugers Archiv: European Journal of Physiology*, **459**, 47–54.

Santos, K. O., Costa, J., Spagnol, K. L., Nornberg, B. F., Lopes, F. M., Tesser, M. B., & Marins, L. F. (2020). The inclusion of a transgenic probiotic expressing recombinant phytase in a diet with a high content of vegetable matter markedly improves growth performance and the expression of growth-related genes and other selected genes in zebrafish. *Aquaculture*, **519**, 734878.

Smith, D. E., Clemencon, B., & Hediger, M. A. (2013). Proton-coupled oligopeptide transporter family SLC15: Physiological, pharmacological and pathological implications. *Molecular Aspects of Medicine*, **34**, 323–336.

Team RDC (2009). *R: A Language and Environment for Statistical Computing*. R Foundation for Statistical Computing, Vienna.

Terada, T., Sawada, K., Irie, M., Saito, H., Hashimoto, Y., & Inui, K. (2000). Structural requirements for determining the substrate affinity of peptide transporters PEPT1 and PEPT2. *Pflugers Archiv: European journal of physiology*, **440**, 679–684.

Torreilles, S. L., McClure, D. E., & Green, S. L. (2009). Evaluation and refinement of euthanasia methods for Xenopus laevis. *Journal of the American Association for Laboratory Animal Science*, **48**, 512–516.

Vacca, F., Barca, A., Gomes, A. S., Mazzei, A., Piccinni, B., Cinquetti, R., Del Vecchio, G., Romano, A., Ronnestad, I., Bossi, E., & Verri, T. (2019). The peptide transporter 1a of the zebrafish Danio rerio, an emerging model in nutrigenomics and nutrition research: Molecular characterization, functional properties, and expression analysis. *Genes & Nutrition*, **14**, 33.

Verri, T., Barca, A., Pisani, P., Piccinni, B., Storelli, C., & Romano, A. (2017). Di- and tripeptide transport in vertebrates: The contribution of teleost fish models. *Journal of Comparative Physiology B, Biochemical, Systemic, and Environmental Physiology*, **187**, 395–462.

Verri, T., Kottra, G., Romano, A., Tiso, N., Peric, M., Maffia, M., Boll, M., Argenton, F., Daniel, H., & Storelli, C. (2003). Molecular and functional characterisation of the zebrafish (Danio rerio) PEPT1-type peptide transporter. *Febs Letters*, **549**, 115–122.

Verri, T., Romano, A., Barca, A., Kottra, G., Daniel, H., & Storelli, C. (2010). Transport of di- and tripeptides in teleost fish intestine. *Aquaculture Research*, **41**, 641–653.

Verri, T., Terova, G., Dabrowski, K., & Saroglia, M. (2011). Peptide transport and animal growth: the fish paradigm. *Biology Letters*, **7**, 597–600.

Viennois, E., Pujada, A., Zen, J., & Merlin, D. (2018). Function, regulation, and pathophysiological relevance of the POT superfamily, specifically PepT1 in inflammatory bowel disease. *Comprehensive Physiology*, **8**, 731–760.

Wada, M., Miyakawa, S., Shimada, A., Okada, N., Yamamoto, A., & Fujita, T. (2005). Functional linkage of H+/peptide transporter PEPT2 and Na+/H+ exchanger in primary cultures of astrocytes from mouse cerebral cortex. *Brain Research*, **1044**, 33–41.

Wang, H., Fei, Y. J., Ganapathy, V., & Leibach, F. H. (1998). Electrophysiological characteristics of the proton-coupled peptide transporter PEPT2 cloned from rat brain. *The American Journal of Physiology*, **275**, C967-C975.

Waterhouse, A., Bertoni, M., Bienert, S., Studer, G., Tauriello, G., Gumienny, R., Heer, F. T., deBeer, T. A. P., Rempfer, C., Bordoli, L., Lepore, R., & Schwede, T. (2018). SWISS-MODEL: Homology modelling of protein structures and complexes. *Nucleic Acids Research*, **46**, W296-W303.

Wickham, H., Averick, M., Bryan, J., Chang, W., D'Agostino McGowan, L., Romain, F., Garrett, G., Hayes, A., Henry, L., Hester, J., Kuhn, M., Pedersen, T. L., Miller, E., Bache, S. M., Müller, K., Ooms, J., Robinson, D., Seidel Paige, D., Spinu, V., … Yutani H. (2019). Welcome to the Tidyverse. *Journal of Open Source Software*, **4**, 1686.

Xu, D., He, G., Mai, K., Wang, Q., Li, M., Zhou, H., Xu, W., & Song, F. (2017). Effect of fish meal replacement by plant protein blend on amino acid concentration, transportation and metabolism in juvenile turbot (Scophthalmus maximus L.). *Aquaculture Nutrition*, **23**, 1169–1178.

Xu, D., He, G., Mai, K., Zhou, H., Xu, W., & Song, F. (2016). Expression pattern of peptide and amino acid genes in digestive tract of transporter juvenile turbot (Scophthalmus maximus L.). *Journal of Ocean University of China*, **15**, 334–340.

Xu, L., Li, Y., Haworth, I. S., & Davies, D. L. (2010). Functional role of the intracellular loop linking transmembrane domains 6 and 7 of the human dipeptide transporter hPEPT1. *The Journal of Membrane Biology*, **238**, 43–49.

Ye, J., Coulouris, G., Zaretskaya, I., Cutcutache, I., Rozen, S., & Madden, T. L. (2012). Primer-BLAST: A tool to design target-specific primers for polymerase chain reaction. *Bmc Bioinformatics [Electronic Resource]*, **13**, 134.

Zhao, D., & Lu, K. (2015). Substrates of the human oligopeptide transporter hPEPT2. *Bioscience Trends*, **9**, 207–213.

Additional information

Open research badges

This article has earned an Open Data badge for making publicly available the digitally-shareable data necessary to reproduce the reported results. The data is available at 10.17605/OSF.IO/563SB.

Data availability statement

The statistical summary document contains data that support the findings of this study. The raw data and fitting parameters

and fitting results are also available here: DOI 10.17605/OSF.IO/563SB.

Competing interests

None.

Author contributions

The experiments were performed in these laboratories: Laboratory of Cellular and Molecular Physiology, Department of Biotechnology and Life Sciences, University of Insubria, Varese (Italy); Department of Biological Sciences, University of Bergen, Bergen (Norway); Research Centre for Aquaculture Systems, National Research Institute of Aquaculture, Japan Fisheries Research and Education Agency, Minami-ise, Mie (Japan); Laboratory of Applied Physiology, Department of Biological and Environmental Sciences and Technologies, University of Salento, Lecce (Italy).

F.V., A.G., K.M., C.R., R.C., A.B., T.V. and E.B.: acquisition, analysis and interpretation of data for the work; F.V., E.B., T.V. and I.R.: design, drafting the work and revising it critically for important intellectual content. All authors have approved the final version of the manuscript; all authors agree to be accountable for all aspects of the work in ensuring that questions related to the accuracy or integrity of any part of the work are appropriately investigated and resolved; all persons designated as authors qualify for authorship, and all those who qualify for authorship are listed.

Funding

I.R. and A.S.G. were supported by the Regional Research Fund West project SalmoFeedPlus (Grant 247978) and Research Council of Norway projects LeuSense (Grant 267626), GUTASTE (Grant 262096) and Gut2Brain 2020 (Grant 311627).

Acknowledgements

The authors would like to thank Drs Anne-Elise O. Jordal, Anders Aksnes and Mali B. Hartviksen for technical assistance during sampling, Dr Anders Aksnes (Cargill Innovation) for providing the fish, and Patrik Tang and Marius Takvam for providing the Atlantic salmon kidney and head-kidney RNA.

Open Access Funding provided by Universita degli Studi dell'Insubria within the CRUI-CARE Agreement.

Present address

Francesca Vacca, Centre for Synaptic Neuroscience and Technology – NSYN@Unige Italian Institute of Technology (IIT), Largo Rosanna Benzi 10, I-16132 Genova, Italy.

Keywords

Di/tripeptide transport(ers), PepT2a, PepT2b, presteady-state currents, Slc15a2a, Slc15a2b, two-electrode voltage-clamp, whole-genome duplication, Xenopus laevis oocytes

Supporting information

Additional supporting information can be found online in the Supporting Information section at the end of the HTML view of the article. Supporting information files available:

Statistical Summary Document
Peer Review History